THEORETICAL NOTES

Note 364

February 1994

A Complete EMP Environment Generated by High-Altitude Nuclear Bursts: Data and Standardization

K.-D. Leuthäuser
Fraunhofer-Institut für Naturwissenschaftlich-Technische Trendanalysen (INT),
Postfach 14 91, 53864 Euskirchen (Germany)
Appelsgarten 2, 53881 Euskirchen (Germany)

ABSTRACT

The EXEMP code described in an earlier Theoretical Note (No. 363) was utilized to compute further numerical data on the HEMP environment. Systematic parameter studies were performed to derive four pulses for different heights of burst and observer positions on ground such that each pulse maximizes one of the four quantities peak amplitude E_{pk} and peak rate of rise $(dE/dt)_{pk}$ of the electric field, energy fluence $1/Z_0 \int E^2(t)dt$ and impulse $\int E(t)dt$. Hence, the envelope to the four wave forms in frequency domain is believed to constitute a greatest lower bound to any single worst case standard wave form. Analytic fits by means of the quotient of the sum of two exponentials (QEXP) are discussed in detail.

1. Introduction

The theoretical elements of the EXEMP code have been presented in a preceding Theoretical Note [1] together with manifold numerical results. This paper attempts to provide additional data, in particular for lower and higher burst points than considered in Ref.1. Because of their significance for the characterization of EMP standard wave forms, particular emphasis will be on rise time, peak rate of rise, duration and maximum field strength of the pulse and their dependence on various other parameters, e.g. height of burst, observer location, gamma yield, pulse shape and average energy of gammas released by the nuclear detonation.

In order to construct a single wave form from the variety of calculated HEMP fields which then could be considered as a worst-case standard pulse for EMP testing and interaction calculations, a few calculated pulses will be selected in such a way that their contribution to a certain part of the frequency spectrum is maximized. Hence, the envelope of these wave forms in frequency domain may provide a greatest lower bound to the Fourier transform of a single standard wave form.

2. EXEMP Code Characteristics

The input of EXEMP requires specification of the following parameters

- gamma yield (kt)
- average gamma energy (MeV)
- number of energy groups of Compton electrons N_e
- number of angular groups of Compton electrons N_n
- observer location in orthogonal curvilinear coordinates with respect to Ground Zero (in units of height of burst)
- minimum time at which EMP calculation starts
- time interval for numerical integration of equation of motion and rate equations
- number of time bins N_t
- height of burst (in km)
- height interval (in km) for the numerical integration of Maxwell equation
- number of height intervals N_h
- geomagnetic latitude.

The quotient of the sum of two exponentials (QEXP) will be used as a standard gamma source function (see Annex A). However, any other normalized wave form could be inserted. QEXP has to be specified by its

- rise time constant α
- decay time constant β.

The total CPU time consumption for a single HEMP pulse is given by the product

$$CPU = C_0 N_e N_n N_h N_t^j$$

where j = 2 if a self-consistent calculation is performed, and j = 1 otherwise.
On a DEC Alpha 4000/300 Workstation, the constant is approximately $C_0 = 2.6 \times 10^{-5}$ s for the FORTRAN version. Hence, for 10 energy and angular groups, respectively, 40 height intervals and 100 time bins. the CPU time amounts to 17 min for a self-consistent and 11 s for a non-self-consistent run. There is also a VAX BASIC version available for which $C_0 = 5.7 \times 10^{-4}$ s on the VAX 4000/300.

Optionally, electron avalanching can be omitted, accelerating the CPU time however only by a few %.

Results include

- magnitude and polarization of electric field as a function of time
- peak electric field E_{pk}
- peak rate of rise $(dE/dt)_{pk}$
- energy fluence and impulse as a function of time
- energy fluence and impulse extrapolated to infinite times
- rise time of electric field (10 - 90%)
- half-width of the pulse (width at $E_{pk}/2$)
- pulse duration (width at $E_{pk}/10$).

Electric field data output in the gamma deposition layer (5 to 70 km above ground) is optionally provided.

3. Numerical Results

The following results were obtained for a QEXP type gamma source function (see Annex A)

$$S(t) = \frac{1}{N_0} \frac{1}{e^{-\alpha t} + e^{\beta t}} \tag{1}$$

where N_0 is the normalization factor.
In the limit $\alpha \to \infty$, Eq. (1) degenerates to a decaying step function (DSF)

$$S(t) = \theta(t)\, \beta\, e^{-\beta t} \tag{2}$$

where θ (t) denotes the unit step function.
A decay time coefficient of $\beta = 0.1/ns$ will be used throughout this paper. A rise time coefficient of $\alpha = 1$ /ns is assumed as Rossi-alpha of the nuclear weapon in Figs. 1 to 12. Because modern nuclear devices may produce even shorter rise times, the parameters of realistic EMP fields will be somewhere between QEXP and the limiting DSF curves which are also presented.

In Figs. 1 to 8, the calculations are performed for a nuclear burst at HOB = 100 km. Except for Fig. 7, an average gamma energy of $E_\gamma = 2$ MeV is assumed. As shown in [1], a multi-group calculation has no significant influence on the numerical results. Except for Figs. 6 and 7, the gamma yield of the bursts is $Y_\gamma = 10$ kt.

Fig.1 shows the variation of the peak electric field-strength along the meridian through Ground Zero for a height of burst HOB = 100 km. Maximum values are reached southward of GZ at a distance between $y_0 = -(1.5 \text{ to } 1.8) \times \text{HOB}$.[1)]

The associated energy fluence

$$W_\infty = \frac{1}{Z_0} \int_{-\infty}^{+\infty} E^2(t)dt \tag{3}$$

is shown in Fig. 2.

---

1 Orthogonal curvilinear coordinates are introduced at Ground Zero with x_0 in eastward and y_0 in northward directions, respectively.

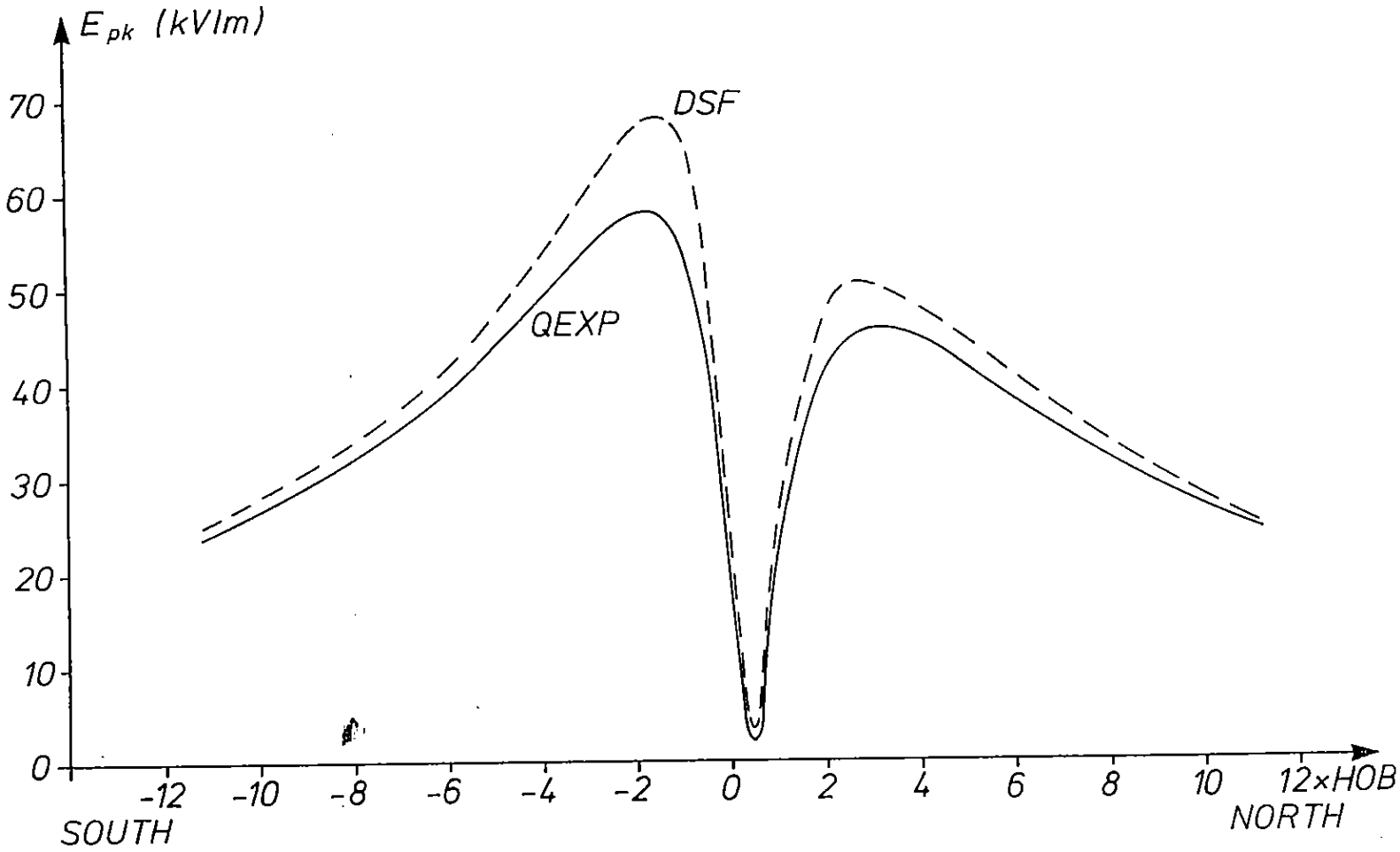

Fig.1 Peak electric field magnitude along the geomagnetic meridian through GZ for Y_γ = 10kt at HOB = 100km. To illustrate the dependence on the gamma source function, calculation were performed both for a QEXP (α = 1 ns^{-1}) and a decaying step function (DSF).

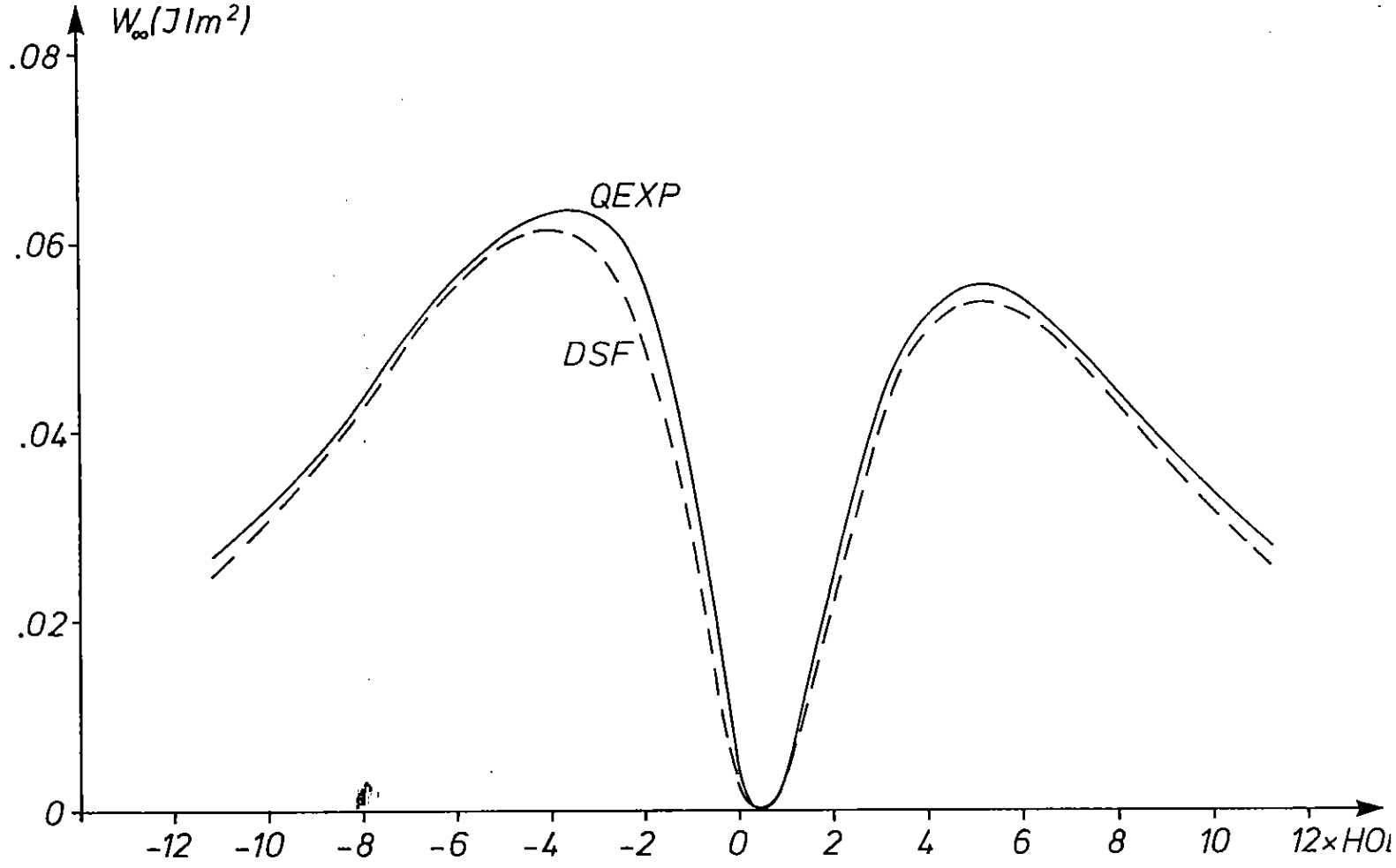

Fig.2 Energy fluence along the geomagnetic meridian through GZ (for further specification see legend of Fig. 1).

Fig. 3 presents the variation of the peak rates of rise with y_0 which for HOB = 100 km attain their maximum values between y_0 = -1.6 HOB and y_0 = -0.7 HOB for the QEXP and the DSF pulse, respectively. The results for the delta function gamma pulse are also shown for comparison. Though not very realistic, they may be considered as an absolute worst case from a computational point of view.

It should be noticed that the peak rate of rise at Ground Zero which sometimes is considered to be decisive for the rise of a worst case HEMP is less than a factor of two as compared with the maximum peak rate of rise.

Figs. 4 and 5 depict the associated rise times T_r (i.e. the time interval between .1 E_{pk} and .9 E_{pk}) and $T_{1/2}$ (i.e. the half-width at .5 E_{pk}), respectively. However, because T_r is only a relative quantity not taking the absolute field amplitude into account, the peak rate of rise plays a more fundamental role for EMP standard considerations.

Figs. 6 and 7 show rise time and half-width of the EMP as a function of the gamma yield of the nuclear detonation at the observer position of maximum peak electric field. The little spike in the QEXP curve of Fig.6 is explained by saturation, i.e. E_{pk} acquires a maximum around a gamma yield of 20 kt as can be seen from the associated E_{pk} values along the curve.

Fig. 8 shows that a variation of the average energy gamma E_γ has practically no influence on the rise time. There is however a considerable increase of E_{pk} and $(dE/dt)_{pk}$ with increasing E_γ. The two curves for the QEXP (α = 1 ns^{-1}) and DSF gamma source function, respectively, refer to an observer position for which E_{pk} (upper curve) and $(dE/dt)_{pk}$ (lower curve) are maximized. Saturation is achieved only for energies > 6 MeV.

Fig. 9 presents maximum peak electric fields and maximum energy fluences as a function of HOB. For the energy fluence, there is practically no difference between QEXP and DSF because in general the pulse duration is considerably longer than the rise time. The numbers along the E_{pk} curves indicate the observer locations southward of Ground Zero where the maximum peak electric fields are expected. The highest electric field strengths are obtained for a height of burst between 110 and 120. The location of maximum energy fluence varies with HOB, as shown in Fig. 10. Highest values of about 0.1 J/m^2 are obtained for HOB $\approx$ 200 km.

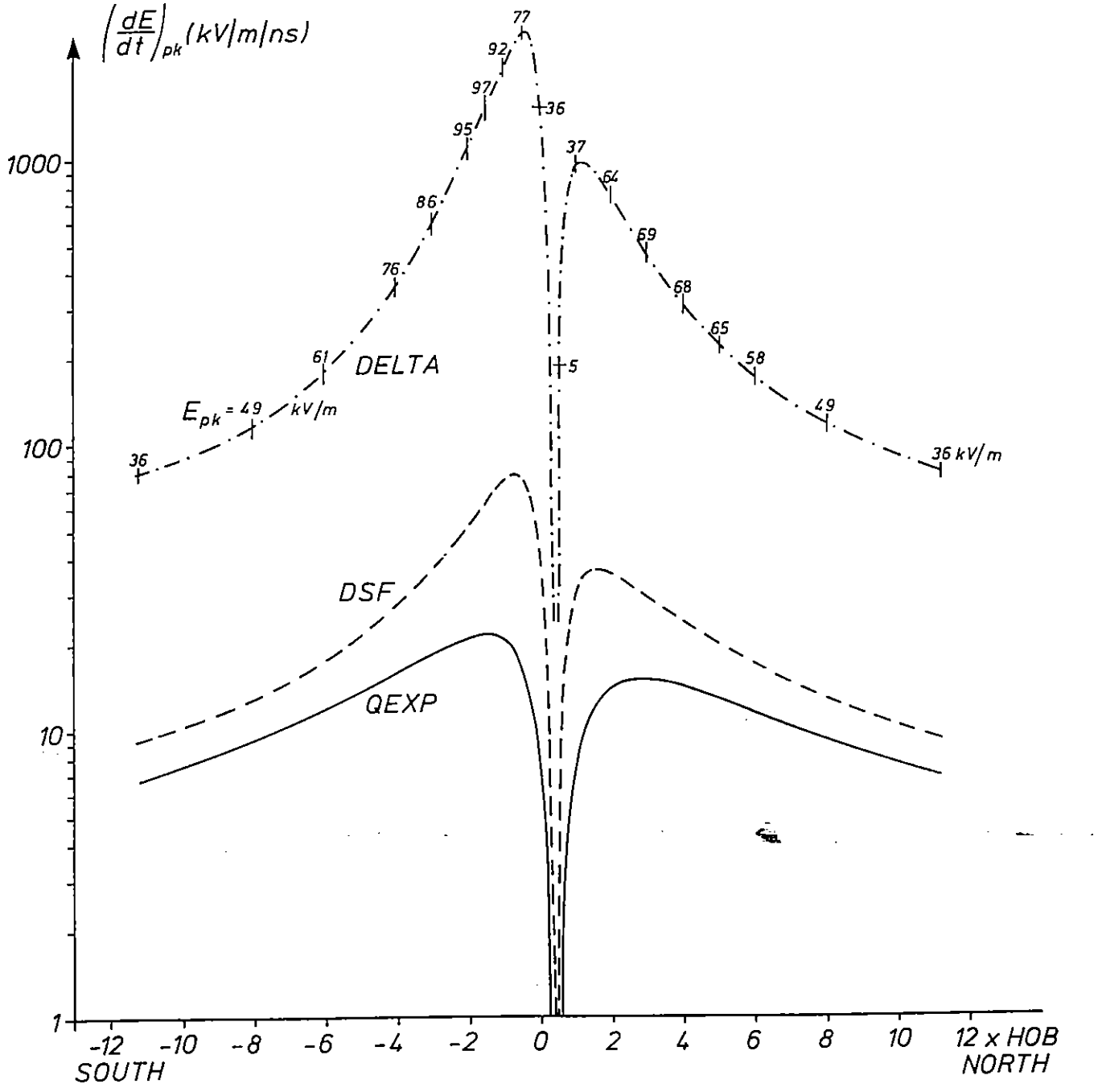

Fig.3 Peak rate of rise of the electric field magnitude along the geomagnetic meridian through GZ (for further specification see legend of Fig. 1). Also shown are results for a delta function gamma source.

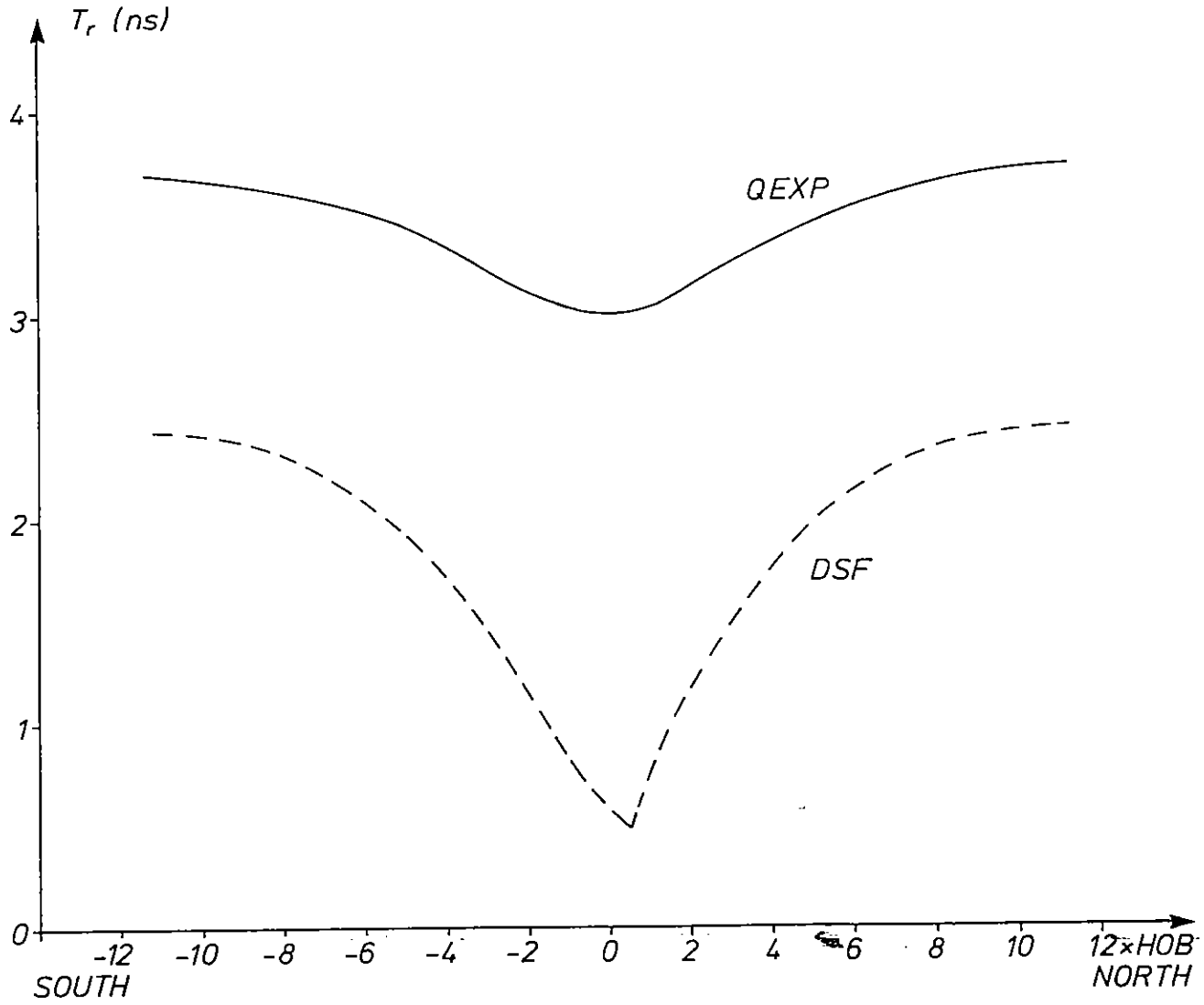

Fig.4 Rise time T_r (10-90%) of the electric field along the geomagnetic meridian through GZ (for further specification see legend of Fig. 1).

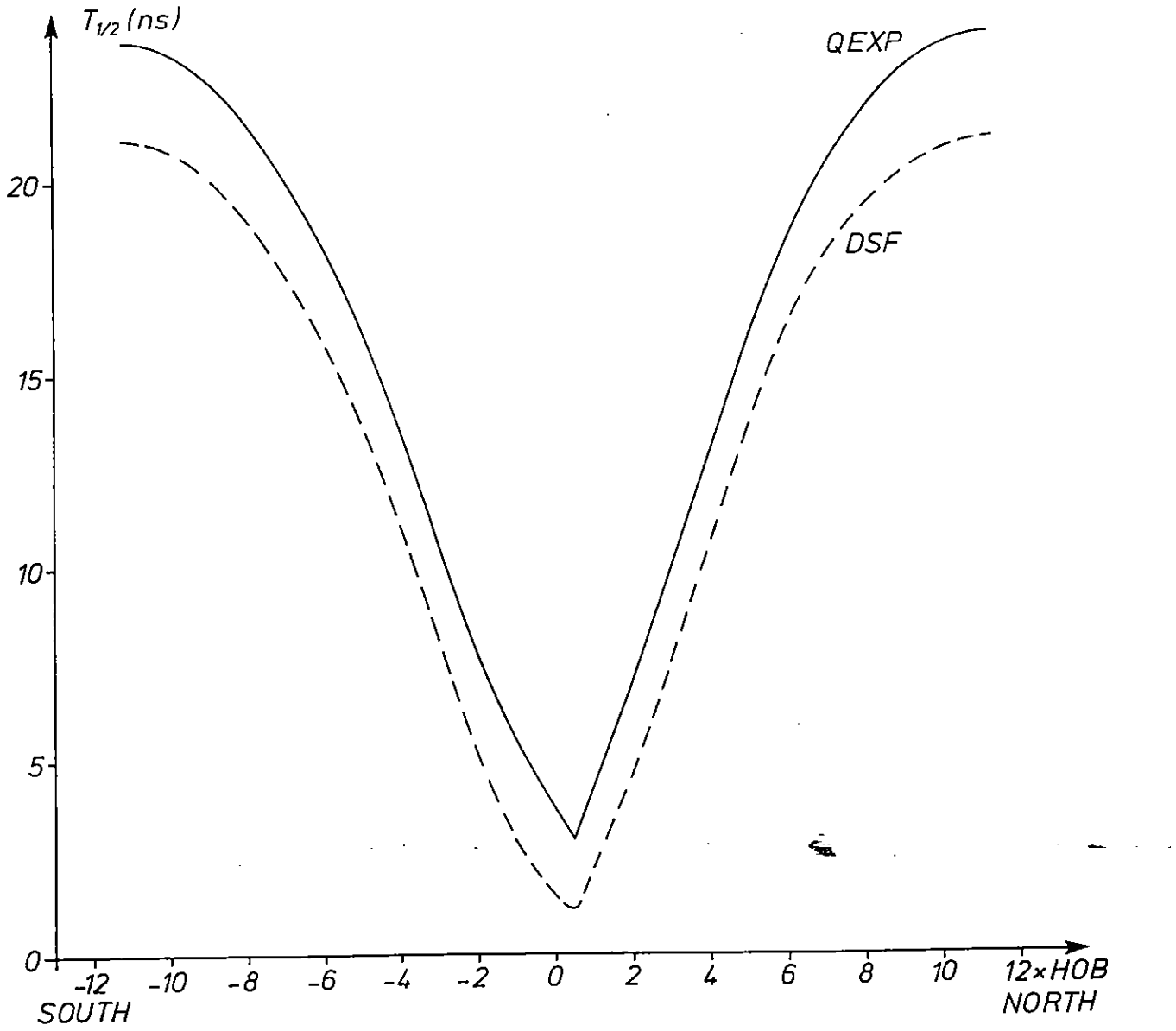

Fig. 5 Half-width of the electric field magnitude along the geomagnetic meridian through GZ (for further specification see legend of Fig. 1).

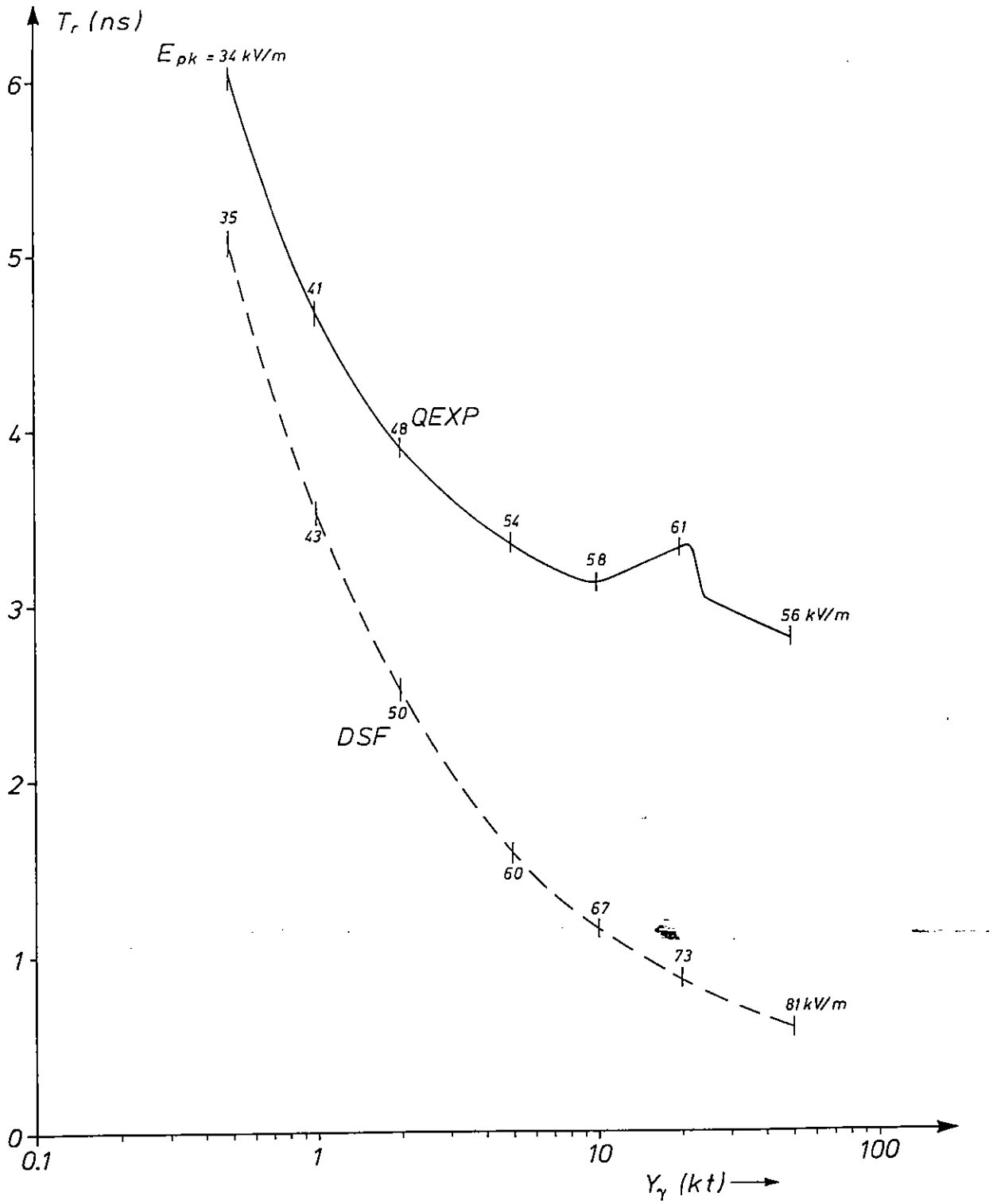

Fig. 6 Variation of rise time with the gamma yield at the observer position of maximum peak electric field as indicated along the curves (HOB = 100 km).

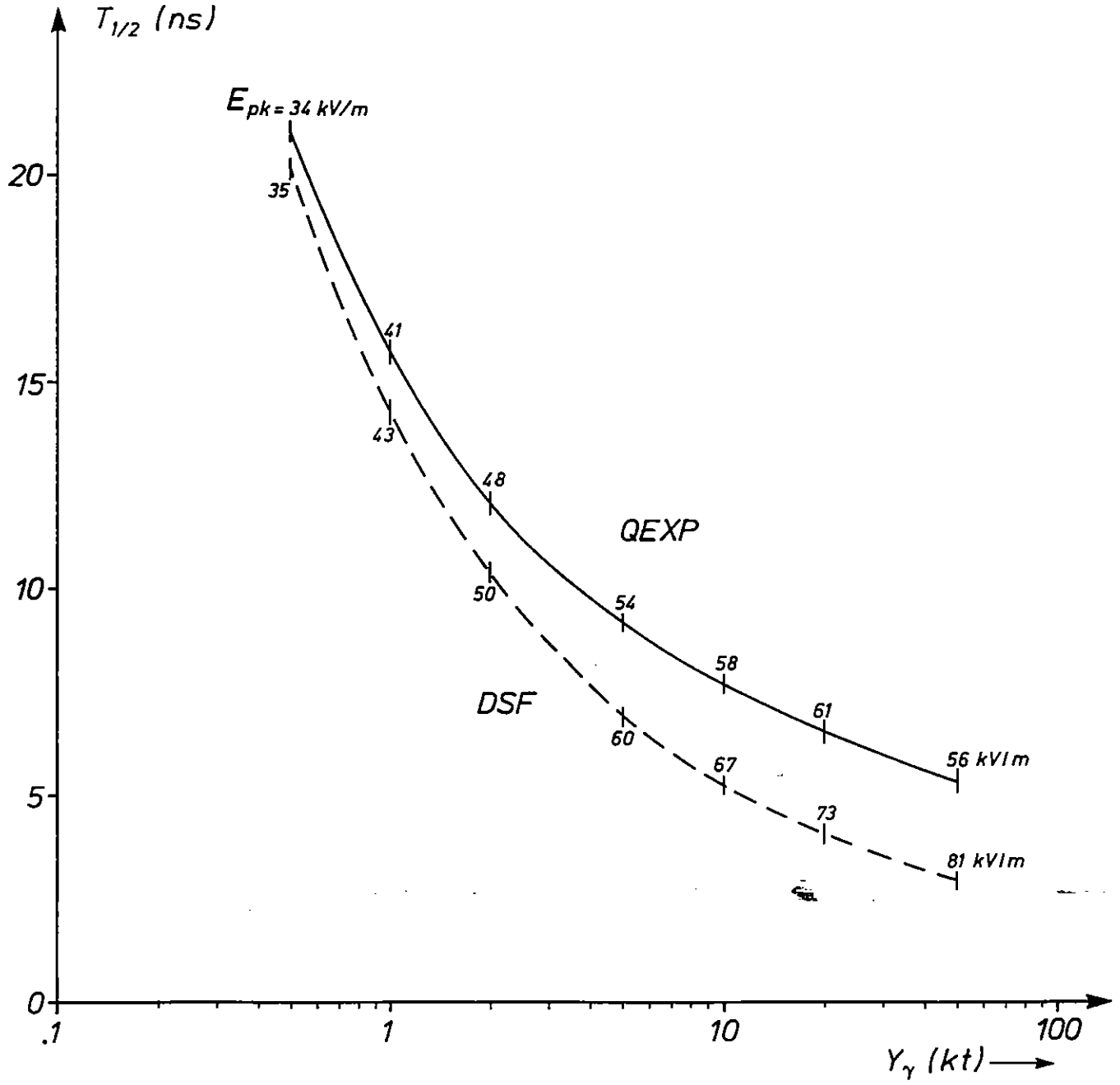

Fig. 7 Variations of half-width with the gamma yield at the observer position of maximum peak electric field as indicated along the curves (HOB = 100 km).

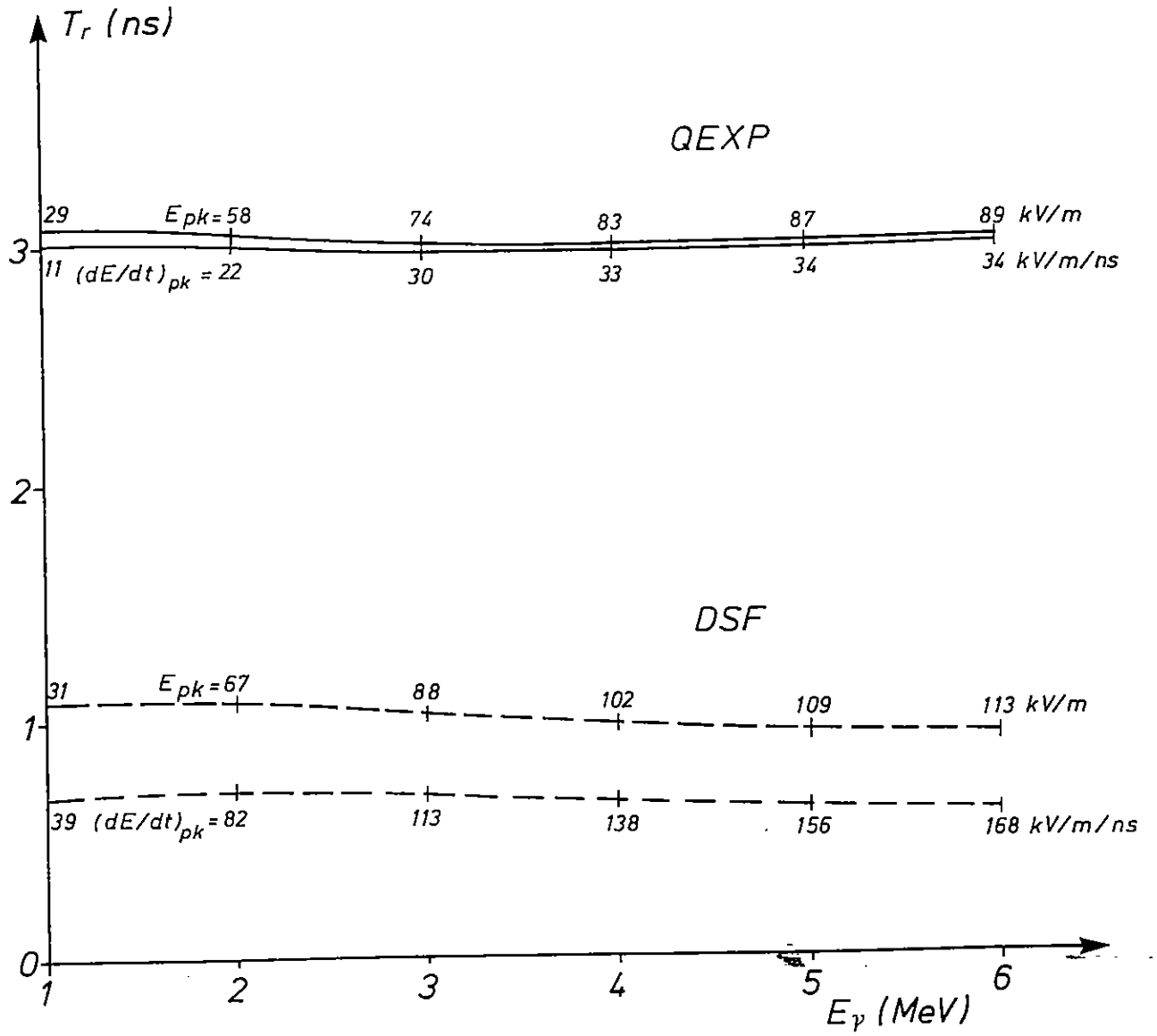

Fig. 8 Variations of rise time with the energy of source gammas at the observer position of peak electric field and peak rate of rise, respectively (HOB = 100 km, Y_γ = 10 kt).

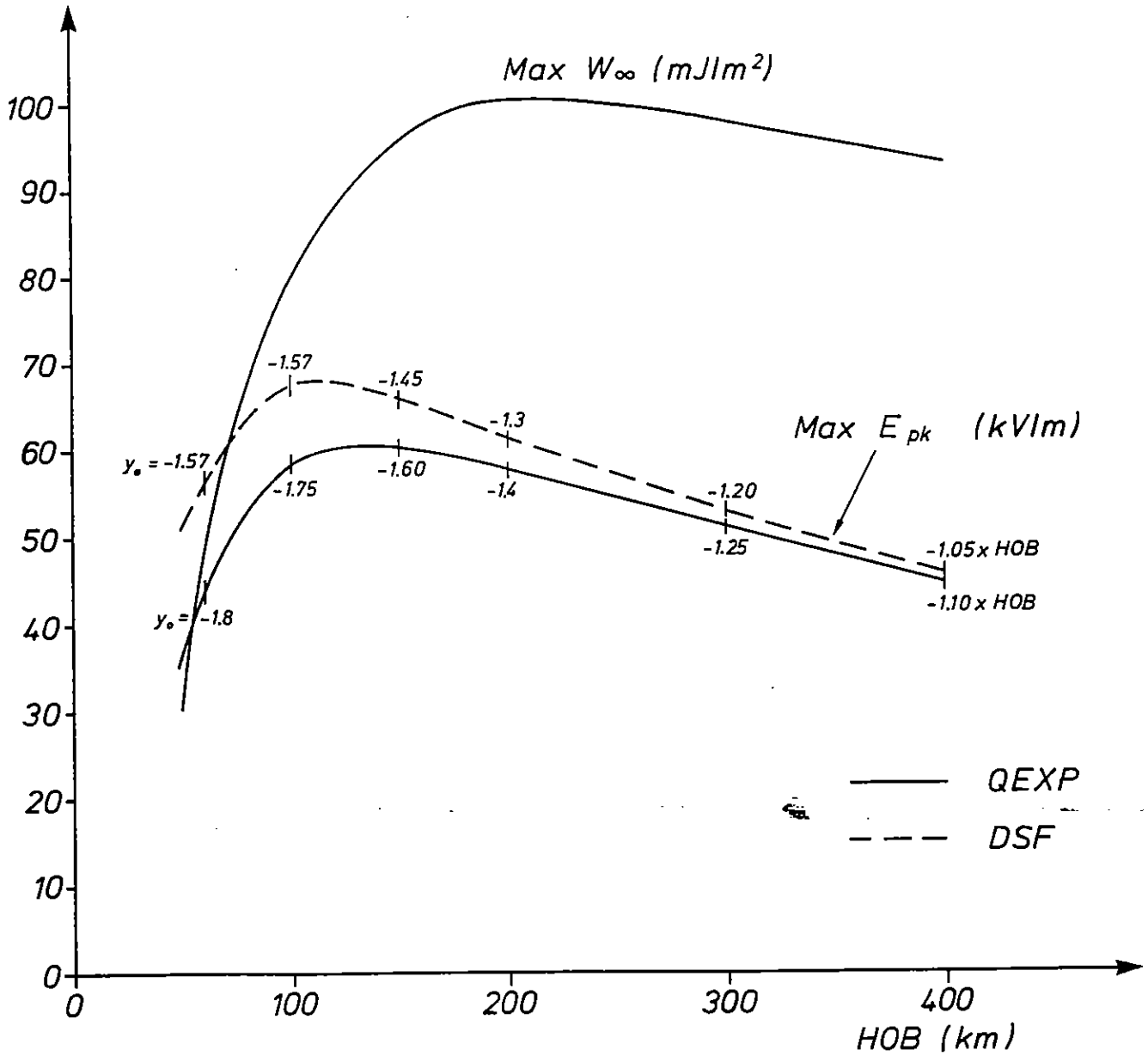

Fig. 9 Variation of maximum peak electric field and maximum energy fluence with height of burst. Numbers along the E_{pk} curves indicate the observer position southward of GZ where the maximum values occur (for W_∞ see Fig. 10).

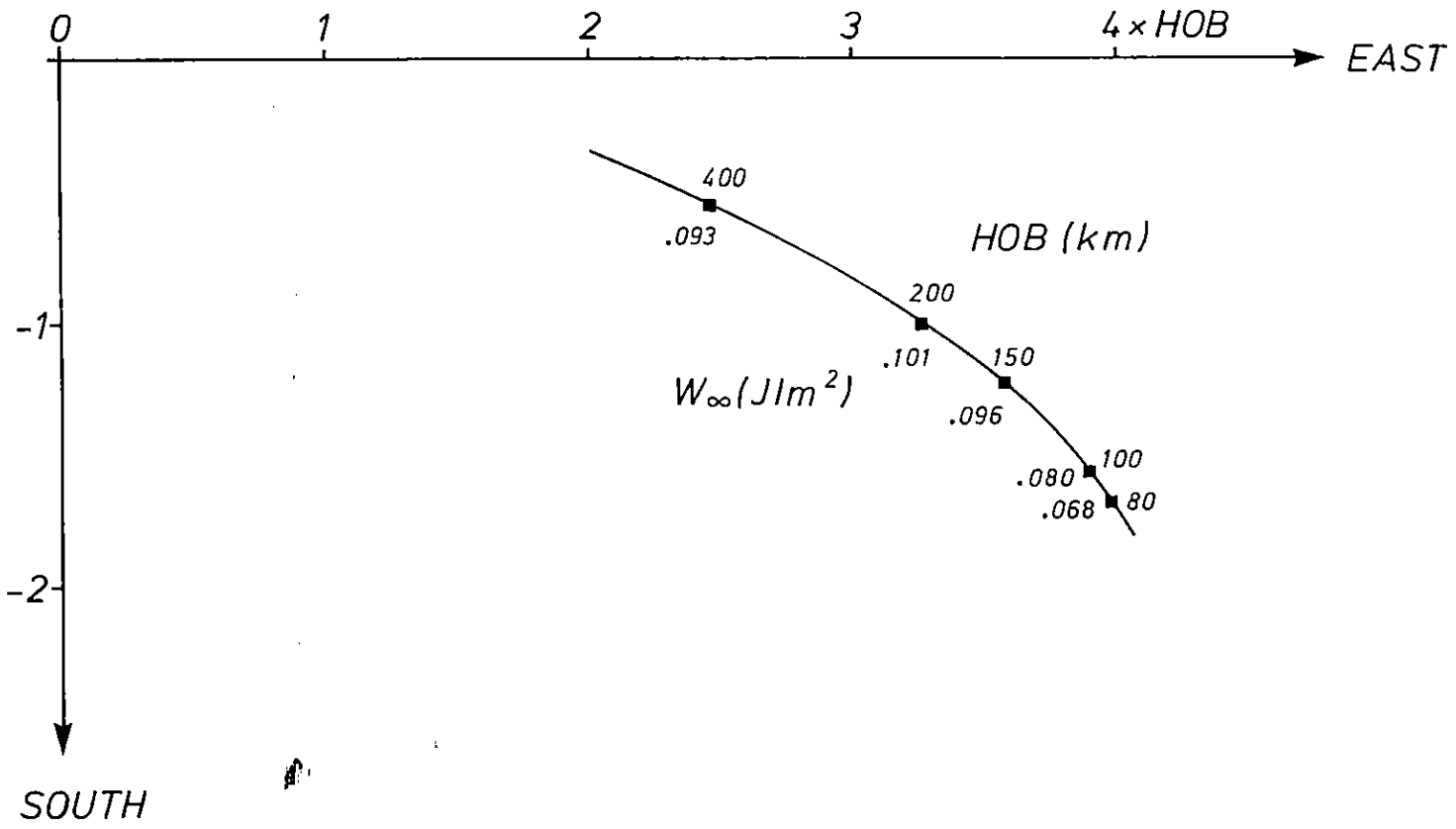

Fig. 10 Observer positions of maximum energy fluence at different heights of burst.

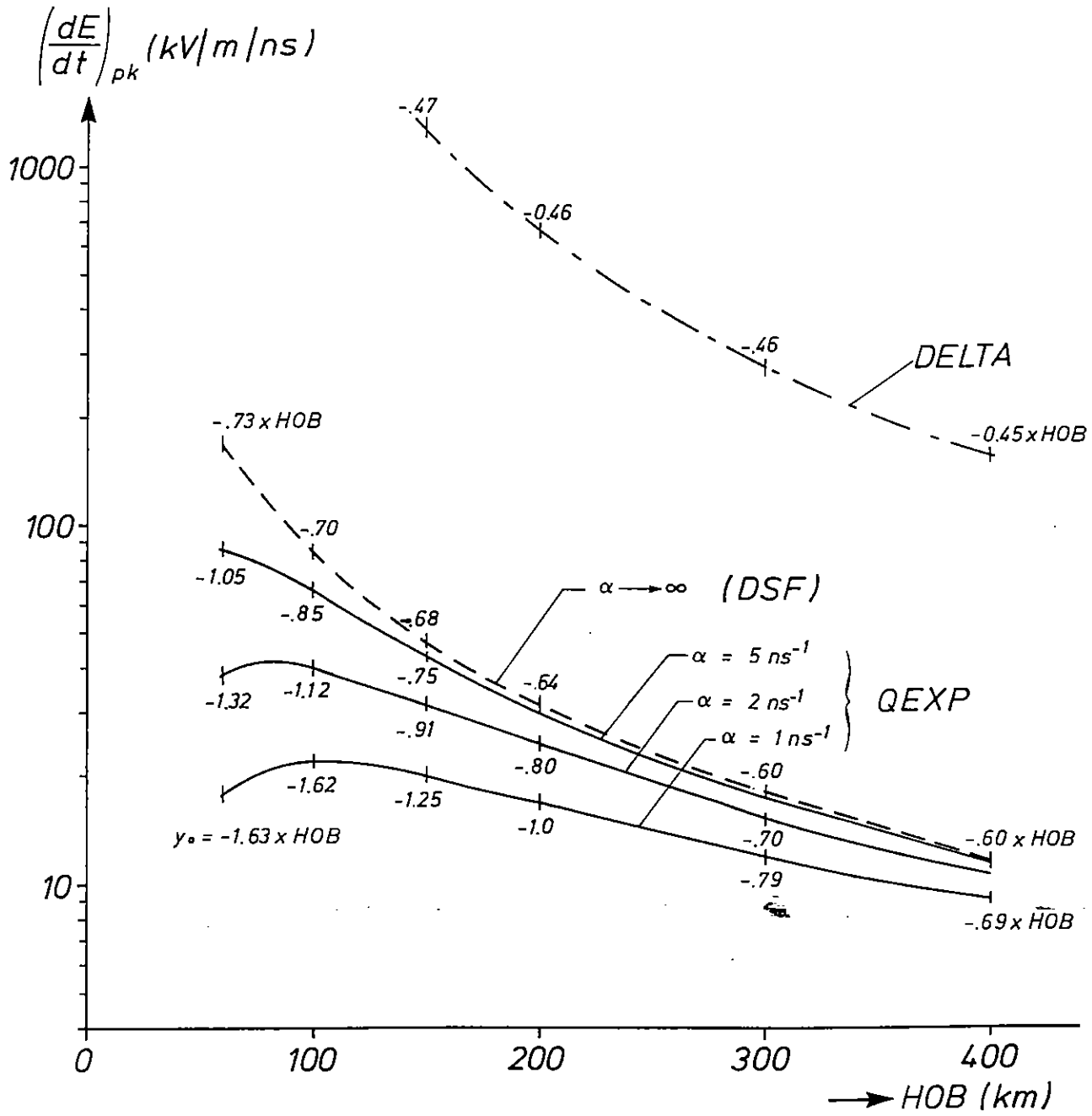

Fig. 11 Variation of maximum peak rate of rise with height of burst. Numbers along the curves indicate the observer positions southward of GZ where the maximum values occur.

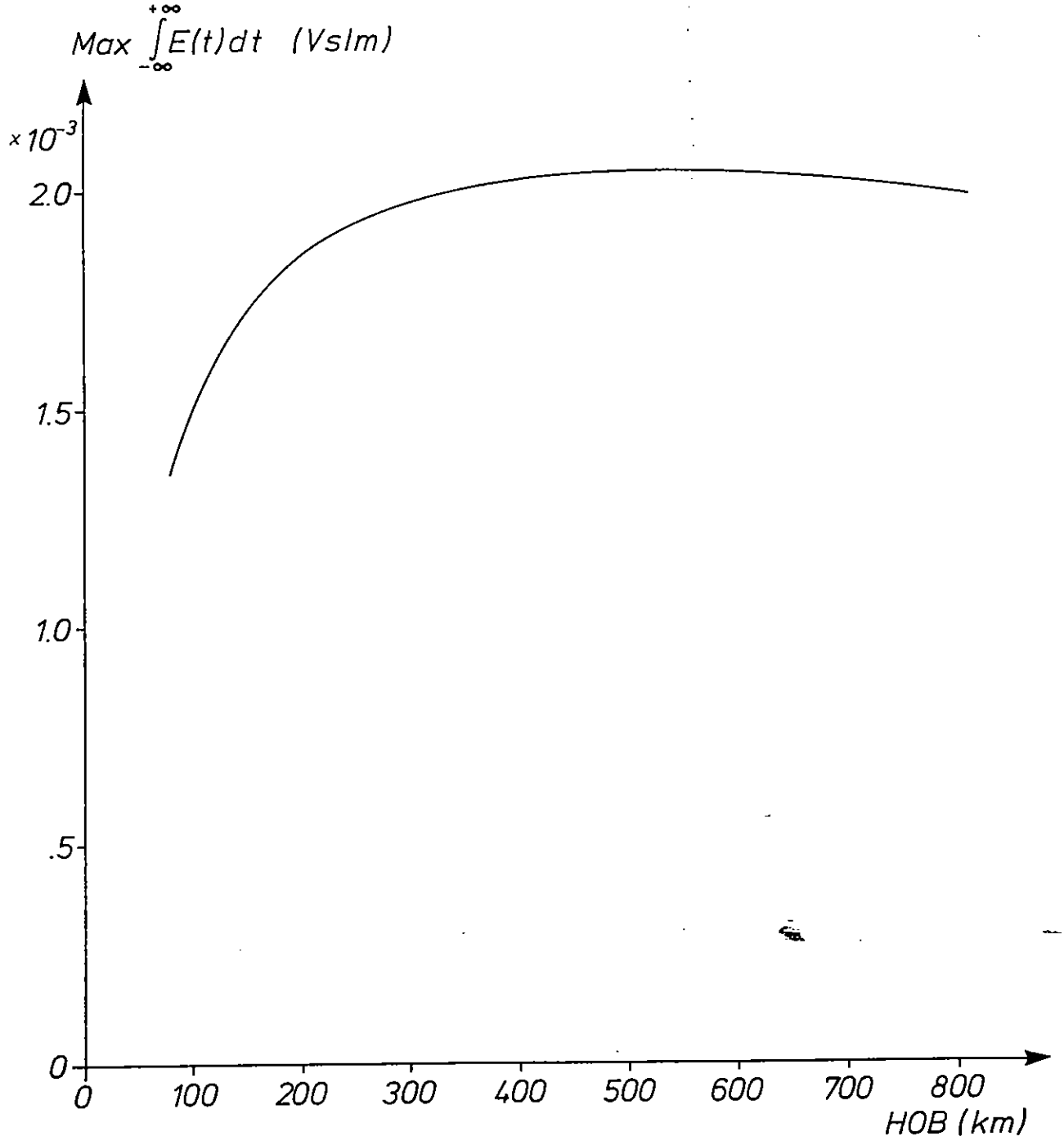

Fig. 12 Variation of maximum impulse with height of burst.

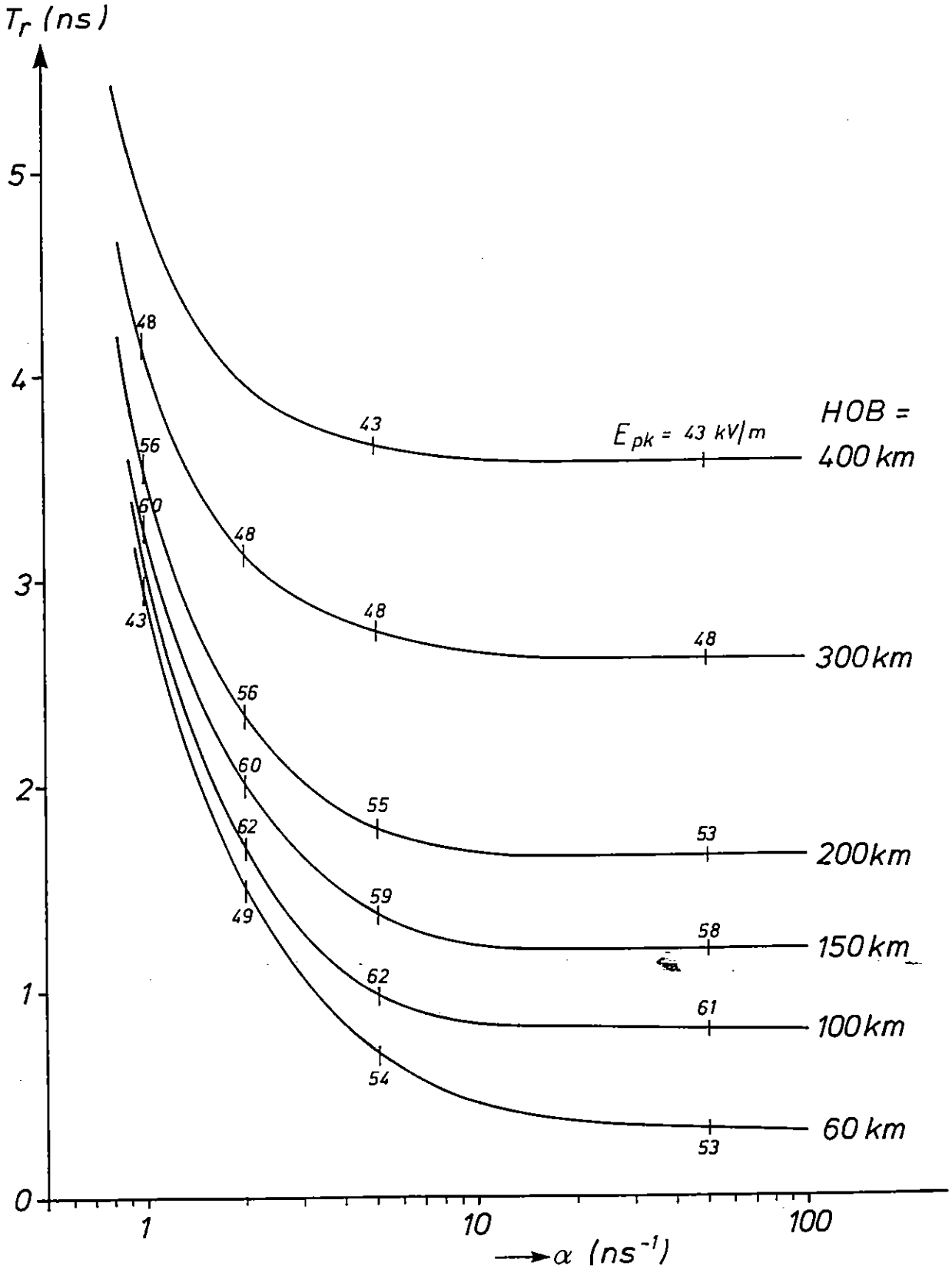

Fig. 13 Variation of rise time with the rise time coefficient α (Rossi-α) of the QEXP gamma source function and HOB at the corresponding locations of maximum peak electric fields.

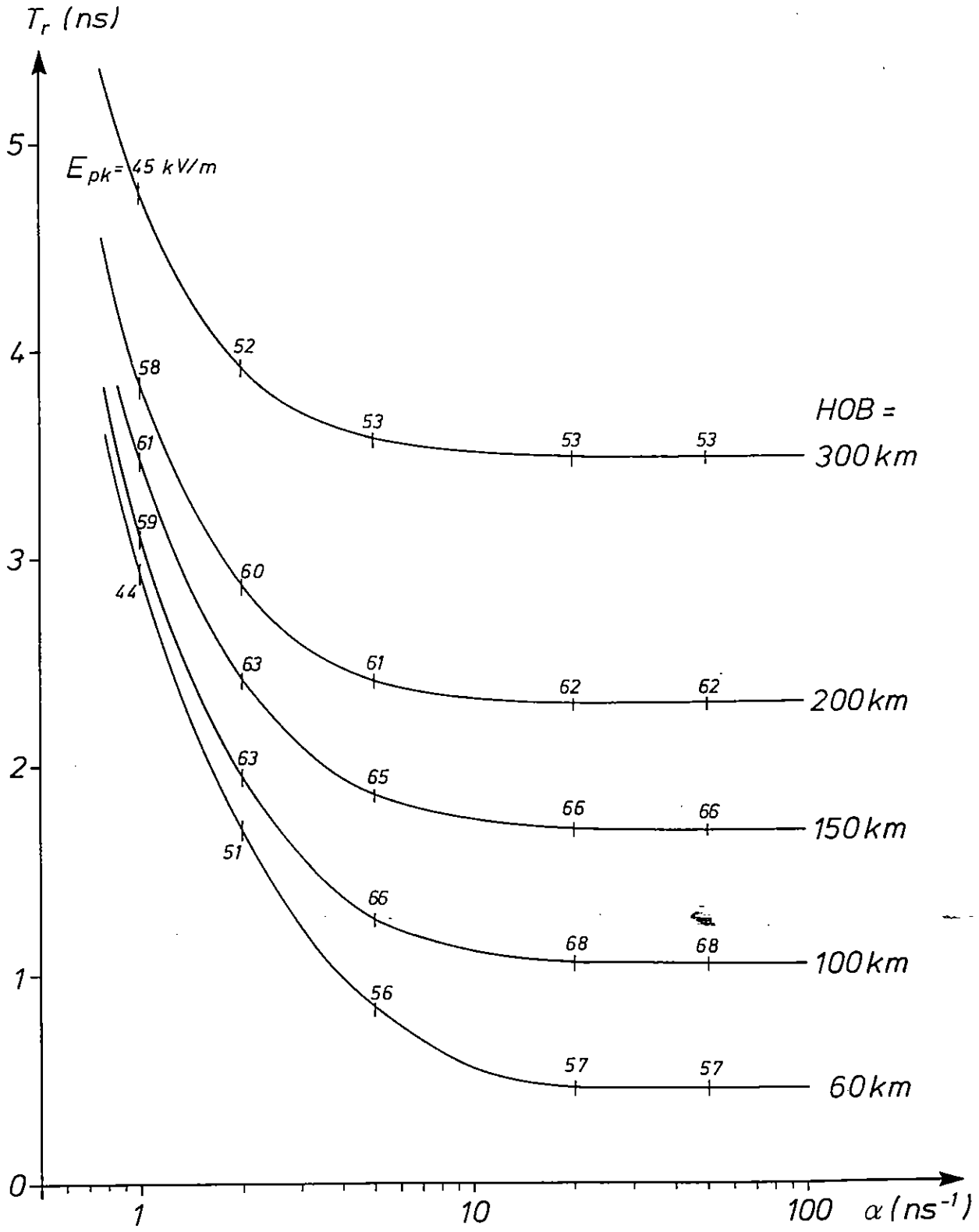

Fig. 14 Variations of rise time with the rise time coefficient α (Rossi-α) of the QEXP gamma source function and HOB at the corresponding locations of maximum peak rate of rise.

Similarly, Fig. 11 shows the variation of the maximum peak rate of rise with HOB for several Rossi-alphas of a QEXP gamma pulse. The numbers along the curves denote the observer position at the particular HOB where $(dE/dt)_{pk}$ takes its maximum. Also shown is the absolute worst case represented by a delta function gamma pulse.

As shown in Fig. 12, the impulse

$$I_\infty = \int_{-\infty}^{+\infty} E(t)dt \tag{4}$$

acquires its maximum of about .002 Vs/m for an HOB of around 600 km. Figs. 17 and 18 indicate a considerable shift of the relative observer location of maximum impulse when varying HOB.

Figs.13 and 14 combine the dependence of T_r on HOB and Rossi-α. In Fig. 13 the observer position is such that the peak rate of rise will be maximized, whereas in Fig. 14 the observer position maximizing E_{pk} was chosen. Above $\alpha \approx 10$ ns^{-1}, T_r becomes nearly constant and can no longer be distinguished from the DSF case. Again, the numbers along the curves are the associated peak electric fields.

For the lowest meaningful heigths of burst and very fast rising gamma source pulses (whether they can be realized or not is beyond the scope of this investigation) rise times of as low as 0.3 ns could theoretically be reached.

4. Contour Plots

Contour plots of the peak electric field magnitudes were given in Ref. [1] for HOB = 200 km and in Ref. [2] for HOB = 400 km. In the present paper, contour plots are computed for various characteristic HEMP quantities at the particular heights of bursts where they attain their maximum values. All contour plots were obtained for a Rossi-α = 5 ns^{-1}.

Fig. 15 shows the contours of peak rate of rise $(dE/dt)_{pk}$ at HOB = 60 km. Maximum rate of rise is 85 kV/m/ns for the observer position y_0= -1.05 HOB = -63 km southward of GZ (see Fig. 11). Curve parameters are in terms of Max $(dE/dt)_{pk}$. At horizon (i.e. the tangent radius),

$(dE/dt)_{pk}$ has decreased to about 14 kV/m/ns. Only 10% of the total area of 660 km^2 are covered with fields with $(dE/dt)_{pk} \geq 0.5$ Max $(dE/dt)_{pk}$. (See Fig. 17 for more information).

Fig.16 shows contours of E_{pk} at HOB = 115 km. The maximum peak electric field is 67 kV/m at y_0 = -1.51 HOB = -174 km. Curve parameters are in terms of Max E_{pk}. At horizon, E_{pk} decreases to 0.4 × Max E_{pk} = 27 kV/m. The area portions with E_{pk} greater than a given fraction of Max E_{pk} can be taken from Fig. 17.

Fig. 18 is a contour plot of the energy fluence for HOB = 200 km where a maximum of 0.1 Joule/m^2 is reached at the observer location x_0 = 3.25 HOB, y_0 = -1.0 HOB in orthogonal curvilinear coordinates. The curve parameters are in Millijoule/m^2. As for the peak electric fields, the energy fluence decreases by a factor of 2 from its maximum value when approaching the horizon, not by a factor of 4, because the pulse duration at horizon is approximately twice the duration at the location of maximum peak electric field.

This behavior is also reflected in the impulse contour plots as shown in Figs. 19 (HOB = 200 km) and 20 (HOB = 600 km) which indicate only little variance of I_∞ beyond the closer vicinity of Ground Zero. The highest impulse of more then .002 Vs/m can be expected for HOB = 600 km at a distance y_0 = 3.4 ≙ 2000 km northward of Ground Zero (see Fig. 18).

The impulse defined by Eq. (4) is of particular importance because it is identical with the low-frequency limit of the Fourier transform of E(t) (see Annex A).

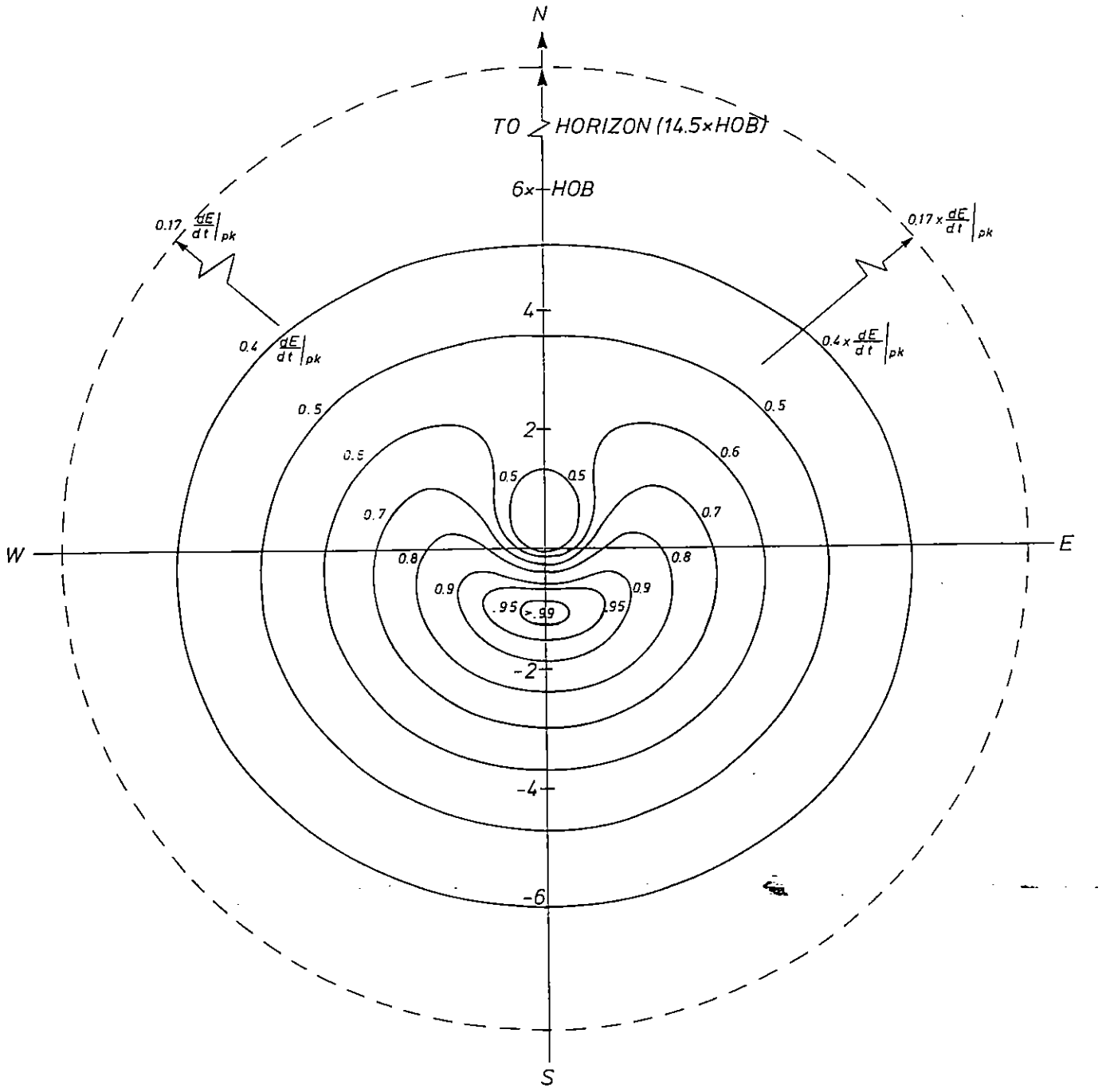

Fig. 15 Contour plot of peak rates of rise (HOB = 60 km, Y_γ = 10 kt, α = 5ns^{-1}). Each contour corresponds to a certain fraction of the maximum peak rate of rise of 84.5 kV/m/ns. The average value over the total area of coverage is 23.5 kV/m/ns.

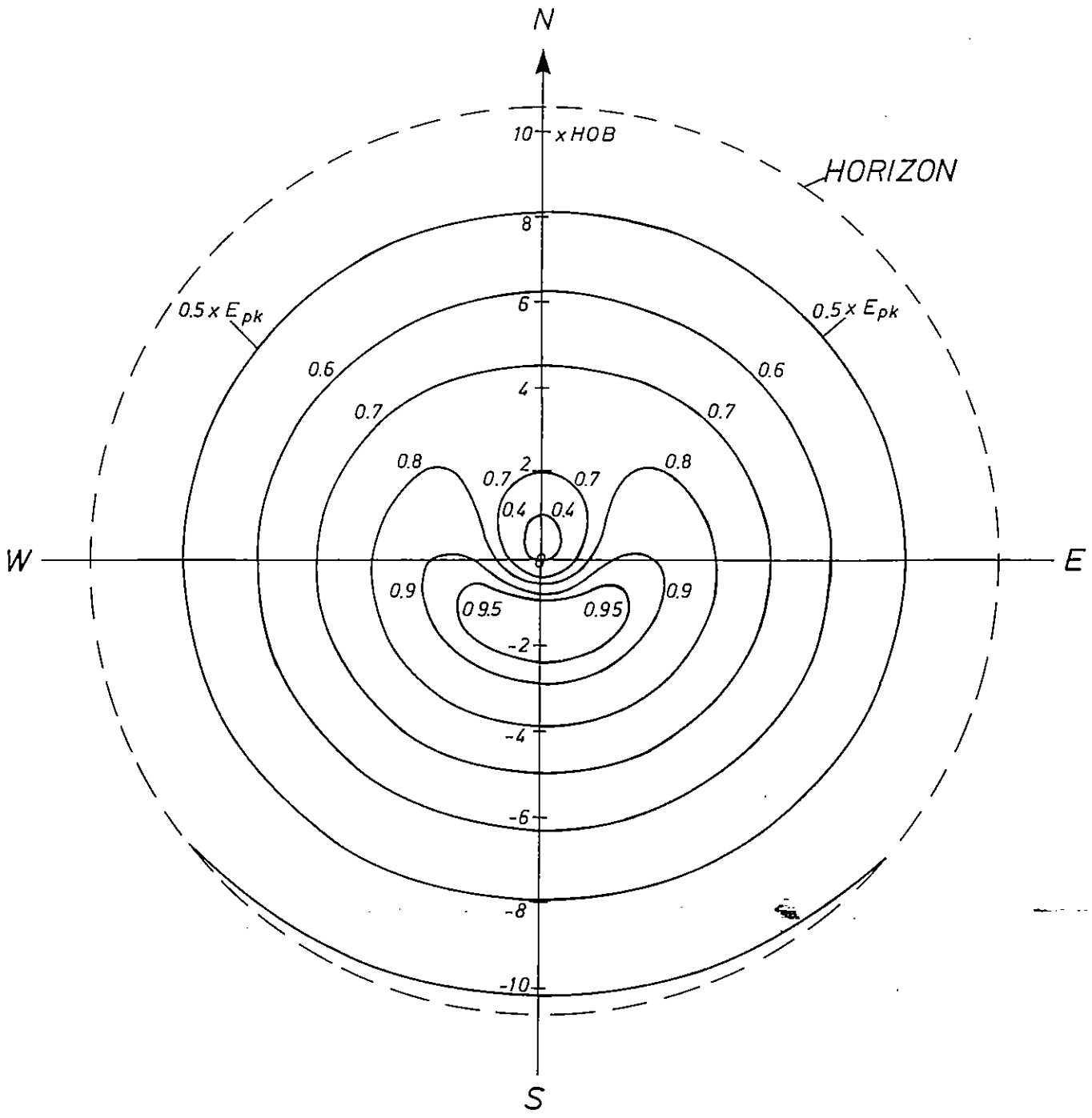

Fig. 16 Contour plot of peak electric fields (HOB = 115 km, Y_γ = 10 kt, α = 5ns^{-1}). Each contour corresponds to a certain fraction of the maximum peak electric field of 67 kV/m. The average value over the total area of coverage is 38.4 kV/m

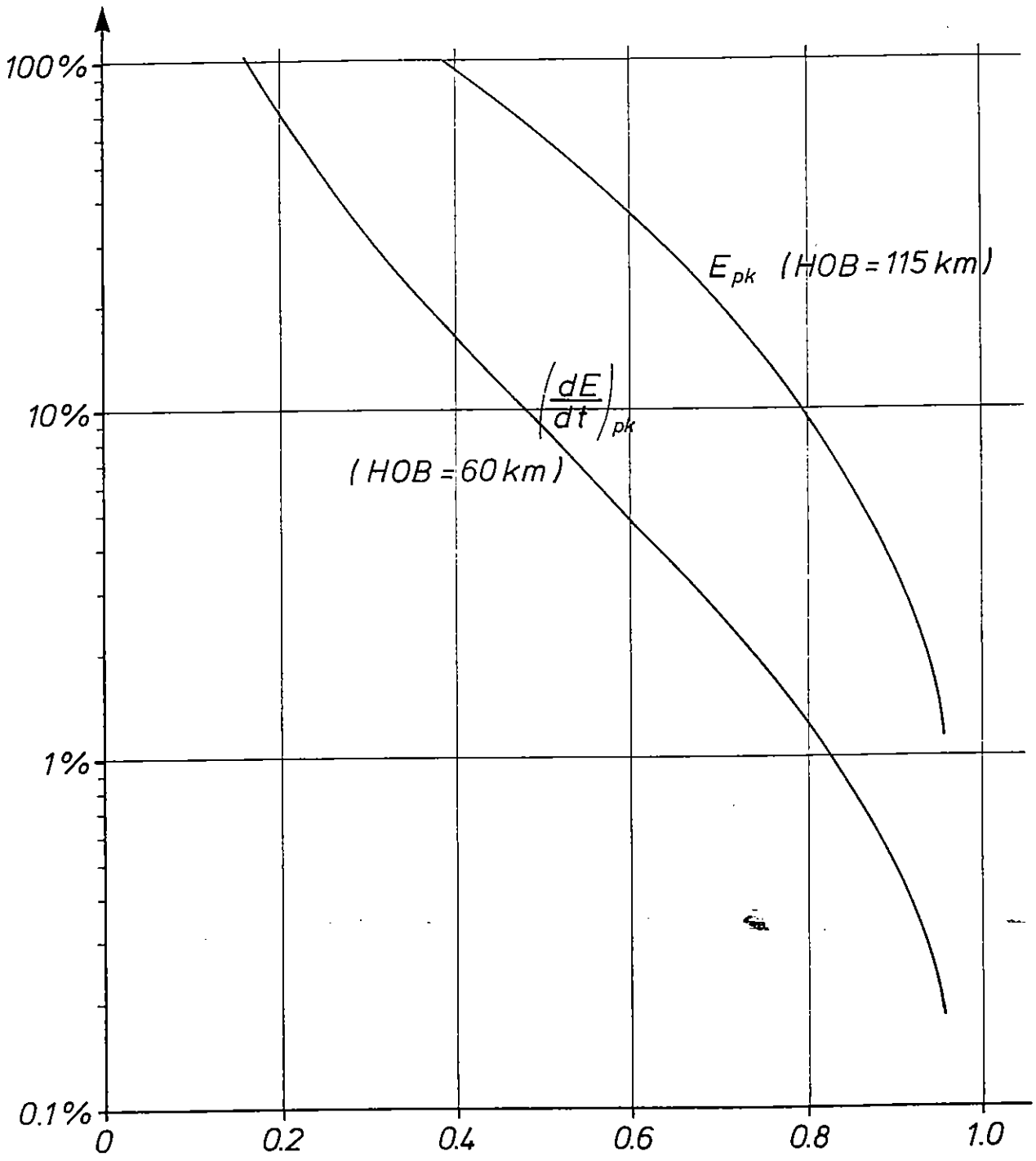

Fig 17 Percentage of the total area of coverage for which peak electric fields and peak rates of rise exceed a given fraction of their respective maximum values.

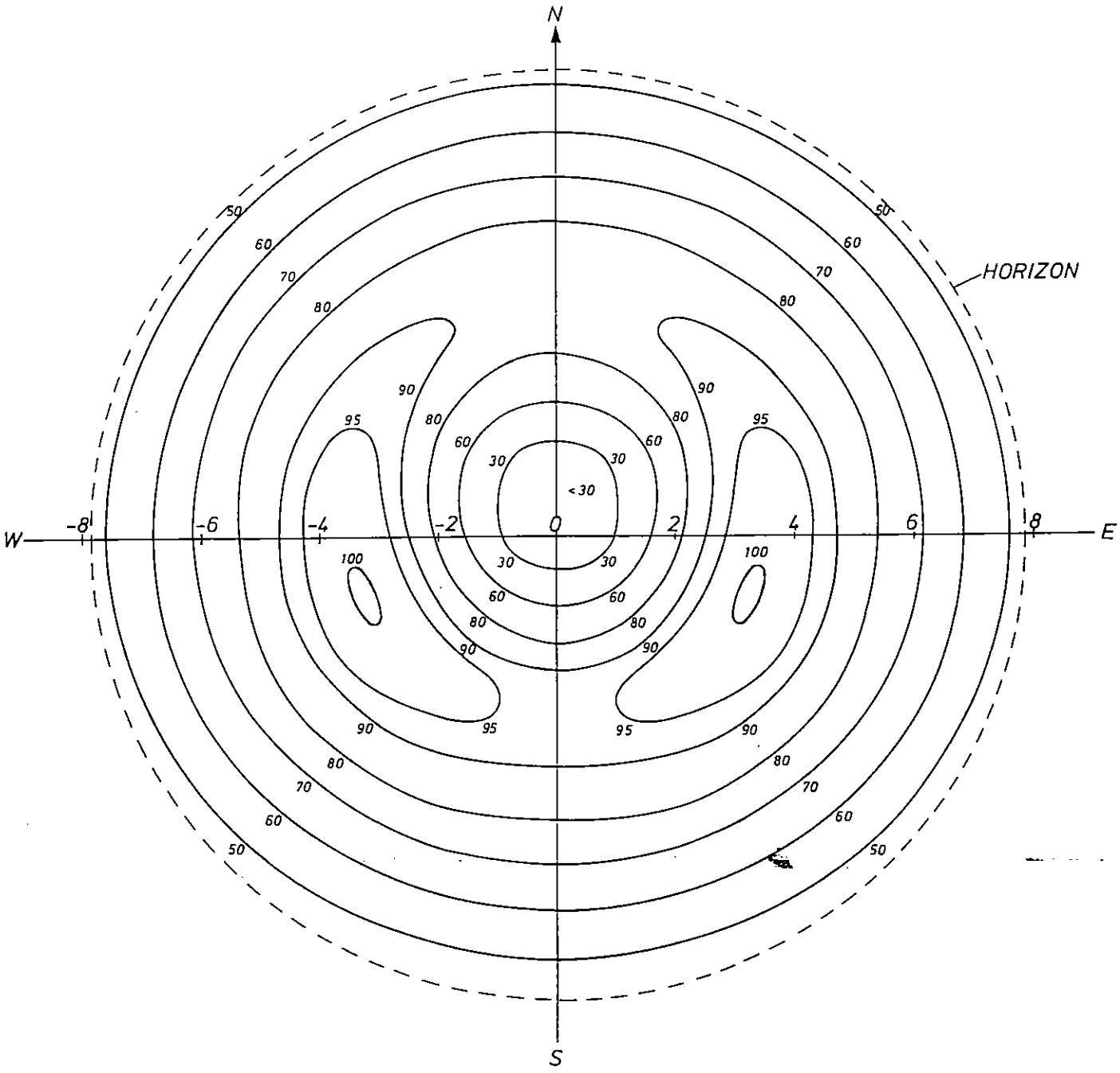

Fig. 18 Contour plot of the energy fluence W_∞ for HOB = 200 km. Numbers on the contours are in units of mJ/m^2.

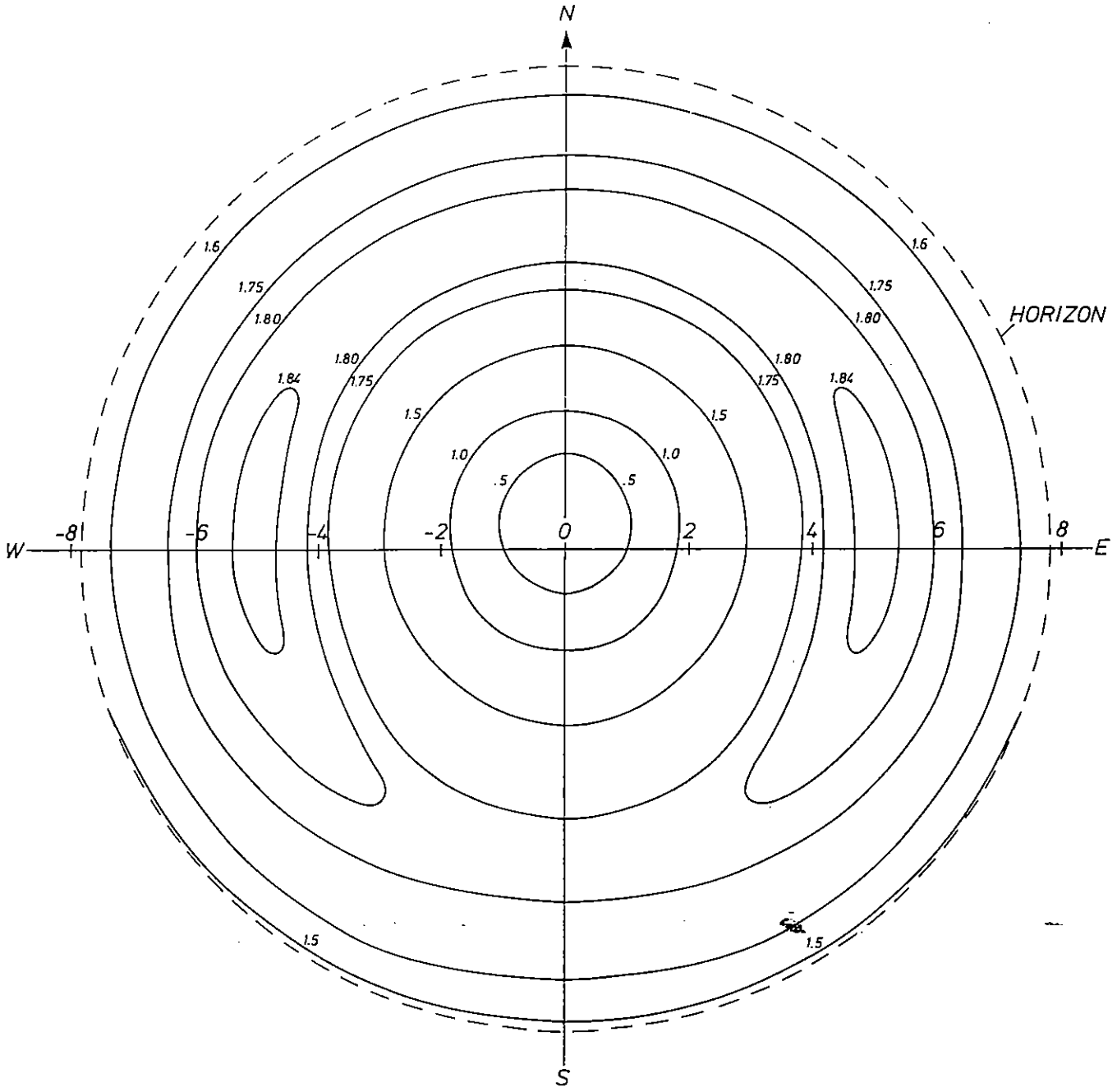

Fig. 19 Contour plot of the impulse I_∞ for HOB = 200 km. Numbers on the contours are in units of 10^{-3} Vs/m.

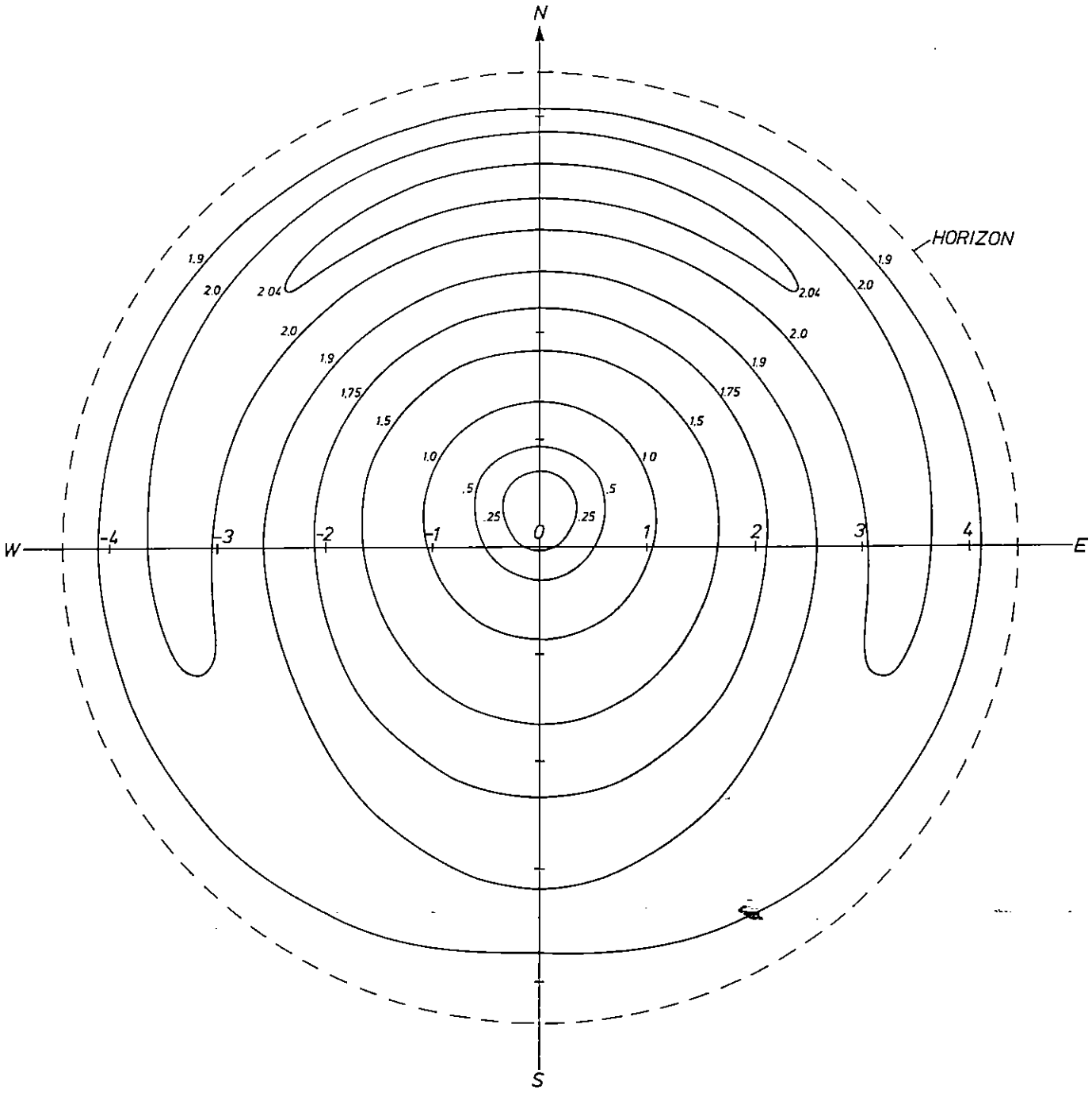

Fig. 20 Contour plot of the of the impulse I_∞ for HOB = 600 km. Numbers on the contours are in units of 10^{-3} Vs/m.

5. Fourier Transforms

Fourier transforms were obtained for four prominent EMP wave forms. for each of which one of the characteristic quantities I_∞, W_∞, E_{pk} and $(dE/dt)_{pk}$ is maximized.*) Each of these pulses maximizes the magnitude of the Fourier transformed electric field in a certain frequency band.

1. The low frequency limit is determined by the impulse I_∞. Therefore. the electric field for HOB = 600 km will be calculated at 1000 km northward of GZ where I_∞ takes its maximum.
2. For lower intermediate frequencies. the pulse of maximum energy will be selected as obtained for HOB = 200 km.
3. For higher intermediate frequencies. the pulse of maximum peak electric field will be chosen as received from a nuclear detonation at HOB = 115 km by an observer located 170-220 km southward of GZ.
4. The high frequency behavior is governd by the EMP peak rate of rise. Therefore. an electric field for HOB = 60 km will be computed at distances of 50 - 100 km southward of GZ where maximum peak rates of rise are expected.

The complete data of the four EMP wave forms are shown in Tables I to IV for different Rossi-alphas. Data obtained for a delta function gamma source are also included for comparison because they constitute an (even though not very realistic) absolute worst case. It is observed that in Tables I and II all data are only weakly dependent on α. On the other hand, for the lower heights of burst $(dE/dt)_{pk}$ and T_r and therefore the high frequency behavior are strongly dependent on α (Tables III and IV).

* The variation of the four characteristic quantities with Y_γ and E_γ related to their nominal values 10 kt and 2 MeV, respectively, is considered in Annex B.

	Delta Function	QEXP $\alpha \rightarrow \infty$	QEXP $\alpha = 5\ ns^{-1}$	QEXP $\alpha = 1\ ns^{-1}$
HOB (km)	600	600	600	600
Location[1]	(0. + 3.4)	(0, + 3.4)	(0. + 3.4)	(0, + 3.4)
E_{pk} (kV/m)	22.9	19.9	19.9	19.9
$(dE/dt)_{pk}$[2]	9.0	1.65	1.64	1.55
T_r (ns)	4.5	13.3	13.3	13.8
$T_{1/2}$ (ns)	59	75	75	75
W_∞ (J/m^2)	0.062	0.061	0.060	0.060
→ I_∞(Vs/m)	1.98×10^{-3}	2.01×10^{-3}	2.05×10^{-3}	2.05×10^{-3}

Table I: Max I_∞ (Pulse # 1)

	Delta Function	QEXP $\alpha \rightarrow \infty$	QEXP $\alpha = 5\ ns^{-1}$	QEXP $\alpha = 1\ ns^{-1}$
HOB (km)	200	200	200	200
Location[1]	(3.25, -1)	(3.25, -1)	(3.25, -1)	(3.25, -1)
E_{pk} (kV/m)	68.0	49.3	49.1	48.0
$(dE/dt)_{pk}$[2]	90	10.9	10.8	9.04
T_r (ns)	1.13	4.20	4.25	5.20
$T_{1/2}$(ns)	7.4	19.1	19.1	19.8
→ W_∞ (J/m^2)	0.083	0.096	0.100	0.094
I_∞(Vs/m)	1.35×10^{-3}	1.56×10^{-3}	1.58×10^{-3}	1.60×10^{-3}

Table II: Max W_∞ (Pulse # 2)

1) orthogonal curvilinear coordinates (x_0, y_0) at GZ in units of HOB
2) kV/m/ns

	Delta Function	QEXP $\alpha \rightarrow \infty$	QEXP $\alpha = 5\ ns^{-1}$	QEXP $\alpha = 2\ ns^{-1}$	QEXP $\alpha = 1\ ns^{-1}$
HOB (km)	115	107	115	122	135
Location [1]	(0, - 1.44)	(0, - 1.45)	(0, - 1.51)	(0, - 1.54)	(0, - 1.61)
→ E_{pk} (kV/m)	96.4	68.3	67.3	64.8	60.3
$(dE/dt)_{pk}$ [2]	1200	59.3	47.7	33.5	20.0
T_r (ns)	0.13	1.08	1.36	1.99	3.28
$T_{1/2}$ (ns)	1.11	4.5	5.0	7.6	5.7
W_∞ (J/m^2)	0.026	0.043	0.047	0.052	0.059
I_∞(Vs/m)	3.5×10^{-4}	5.8×10^{-4}	6.3×10^{-4}	6.7×10^{-4}	7.8×10^{-4}

Table III: Max E_{pk} (Pulse #3)

	Delta Function	QEXP $\alpha \rightarrow \infty$	QEXP $\alpha = 5\ ns^{-1}$	QEXP $\alpha = 2\ ns^{-1}$	QEXP $\alpha = 1\ ns^{-1}$
HOB (km)	60	60	60	80	94
Location [1]	(0, - 0.58)	(0, - 0.71)	(0, - 1.05)	(0, - 1.25)	(0, - 1.63)
E_{pk} (kV/m)	67.7	54.1	54.0	59.1	57.0
→ $(dE/dt)_{pk}$ [2]	12200	165	84.5	42.2	21.9
T_r (ns)	0.009	0.31	0.69	1.57	3.0

Table IV: Max $(dE/dt)_{pk}$ (Pulse #4)

1) orthogonal curvilinear coordinates (x_0, y_0) at GZ in units of HOB
2) kV/m/ns

Table V summarizes the determining quantities of the pulses for $\alpha = 5\ ns^{-1}$, a nominal gamma yield $Y_\gamma = 10$ kt and an average source gamma energy $E_\gamma = 2$ MeV. The variation of the maximum values of E_{pk}, $(dE/dt)_{pk}$, W_∞ and I_∞ with Y_γ and E_γ relative to their nominal values is considered in Annex B.

Pulse #	E_{pk}	$\left(\frac{dE}{dt}\right)_{pk}$	T_r	$T_{1/2}$	$T_{1/10}$	W_∞	I_∞
1	20	1.6	13.3	75	~ 220	.06	**.0020**
2	49	11	4.2	19	80	**.10**	.0016
3	**67**	48	1.4	5.0	27	.05	.0007
4	54	**85**	0.7	3.8	19	.03	.0004

Table V: Characteristics of the pulses 1 to 4

Fig. 21 shows the four selected electric field magnitudes in the time domain with $\alpha = 5\ ns^{-1}$ as 'Rossi-alpha' of the gamma source.

Fig. 22 shows the corresponding electric field magnitudes in the frequency domain.

Because the high frequency behavior is determined by the peak rate of rise of the EMP which, on the other hand, is closely related to the Rossi-alpha of the gamma source pulse, the dependence of the 4th pulse on Rossi-α is particularly shown in Fig. 23. The dashed curve denotes the theoretically attainable high frequency limit for the DSF case (i.e. $\alpha \rightarrow \infty$). It is noted that for $\alpha > 1\ ns^{-1}$ there is practically no substantial difference between the curves up to 100 MHz.

The envelope of the four wave forms in frequency domain can then be considered as a greatest lower bound for the frequency spectrum of a worst case EMP [3].

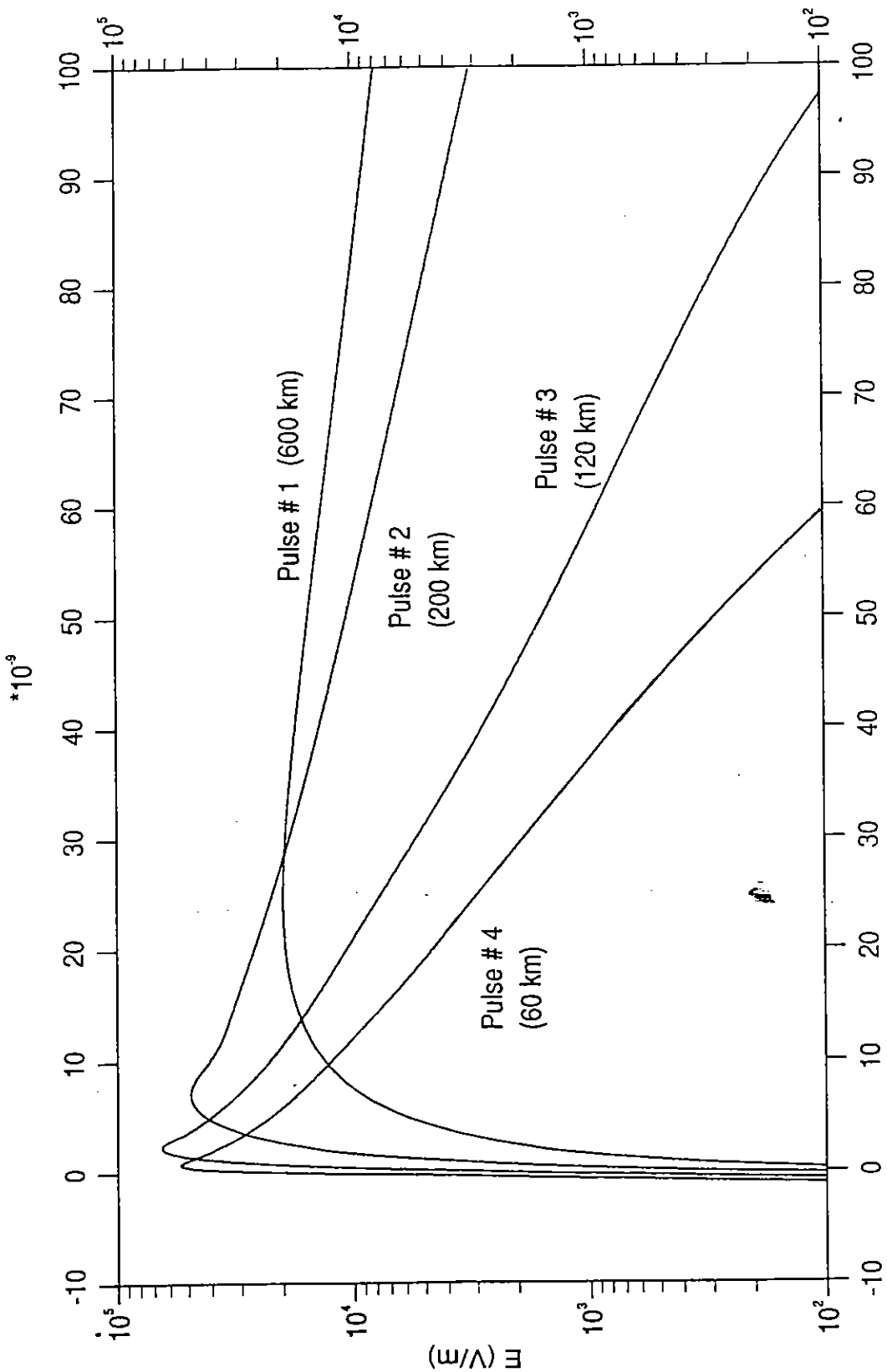

Fig. 21 Total electric field for different heights of burst and observer locations

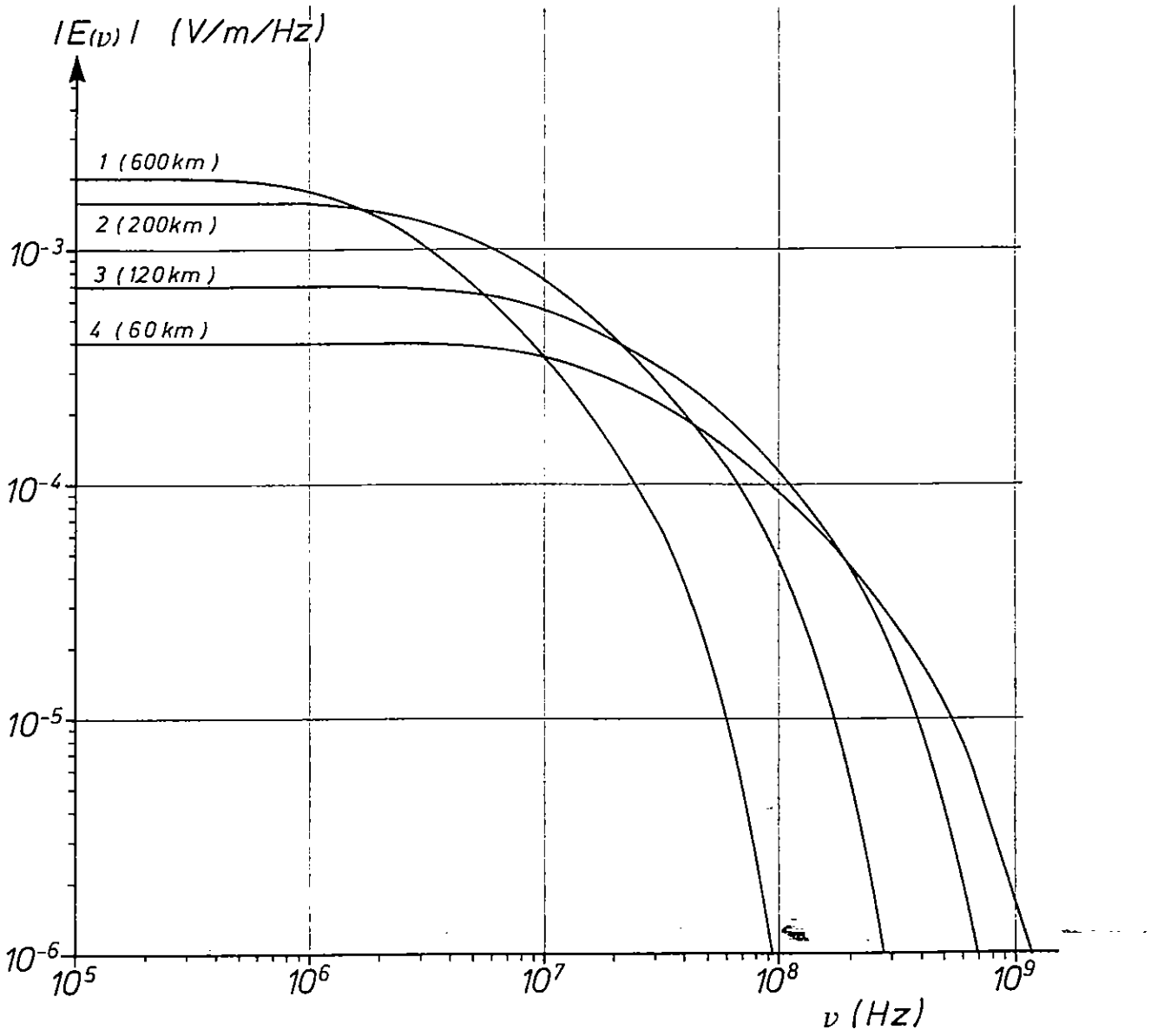

Fig. 22 Amplitude spectrum of the four pulses represented in Fig. 21.

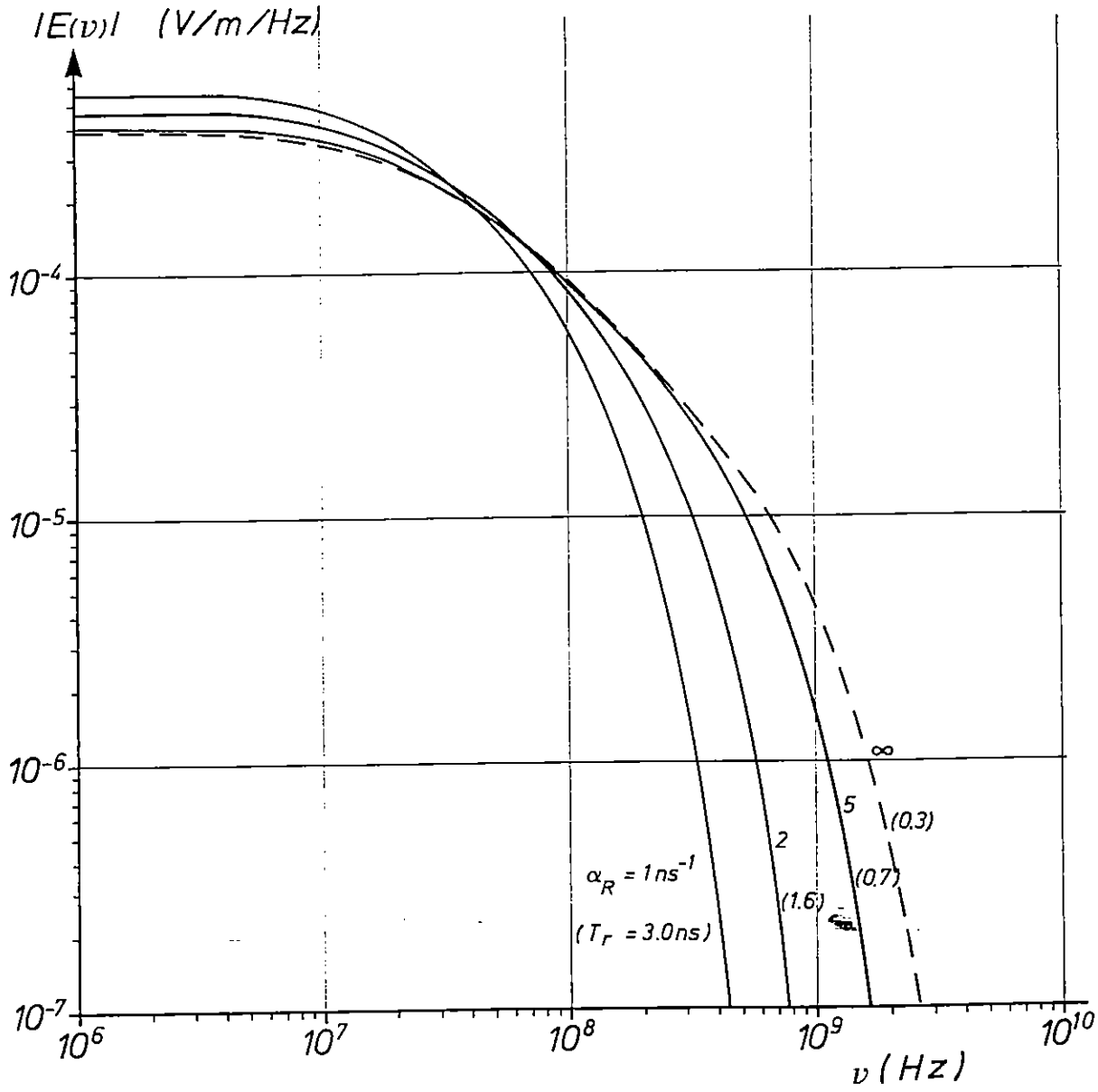

Fig. 23 Amplitude spectrum of four HOB = 60 km bursts calculated for different Rossi-alphas of the gamma source function.

6. Remarks on Standard Wave Forms

For standardization reasons it is desirable to condense the entire knowledge about the variety of actual EMP wave forms into a single analytic expression.
Both the difference of two exponentials (DEXP)

$$E(t) = E_0\left(e^{\alpha t} - e^{\beta t}\right) \tag{5}$$

and the quotient of the sum of two exponentials (QEXP)

$$E(t) = \frac{E_0}{e^{-\alpha t} + e^{\beta t}} \tag{6}$$

are widely used as national and international standards.*)
Numerical examples for the parameters α, β and E_0 based on unclassified EMP data [2] have been presented in [3].
In the following, it will be attempted to derive an independent set of parameters for the QEXP approximation which is in accordance with the results of Sections 3 und 4 and which satisfies the bound condition in frequency domain (Section 5).
Ruling the delta function gamma pulse out for being too unrealistic, it follows from the preceding sections that

$$\begin{aligned} E_{pk} &= 68 \text{ kV/m} \\ I_\infty &= .002 \text{ Vs/m} \\ W_\infty &= .10 \text{ J/m}^2 \\ (dE/dt)_{pk} &< 165 \text{ kV/m/ns (depending on } \alpha_R) \end{aligned} \tag{7}$$

provides a set of worst case EMP characteristics.
It should be noted that in the QEXP fit these data cannot be satisfied simultaneously. As shown in Annex A. the following approximations are obtained from Eq. (6) under the assumption $\alpha >> \beta$:

$$I_\infty \approx \frac{E_0}{\beta}, \qquad W_\infty \approx \frac{E_0^2}{2\beta Z_0} \tag{8}$$

---

* To distinguish between the DEXP/QEXP fits to the electric fields and the QEXP gamma source function, the α of the letter will henceforth be denoted by α_R (i.e. Rossi-α)

Hence

$$W_\infty \approx \frac{E_0}{2Z_0} I_\infty. \tag{9}$$

Thus Eq. (9) could overestimate W_∞ by a factor of 2, if exact fits to E_{pk} and I_∞ are intended. Consistency can only be achieved by introducing additional fit parameters. e.g. by a sum of two QEXP functions

$$E(t) = \sum_{i=1}^{2} \frac{E_{0i}}{e^{-\alpha t} + e^{\beta_i t}} \tag{10}$$

which, however, does not admit an analytic Fourier transform of $E^2(t)$.

Whereas the mismatch of W_∞ and I_∞ affects the low and low intermediate part of the frequency spectrum, the highest frequencies are determined mostly by $(dE/dt)_{pk}$.

QEXP fits with respect to $(dE/dt)_{pk}$, E_{pk} and I_∞ which bound the frequency domain curves in Figs. 22 and 23 are presented in Table VI. Since $(dE/dt)_{pk}$ and the rise time T_r strongly depend on the Rossi-α of the gamma pulse and the QEXP-α coincides with the Rossi-α at the lowest heigths of burst, QEXP fits for different values of α_R are shown. Table VI is completed by QEXP-fit data taken from Ref. [3] based on EMP calculations [2] performed for HOB = 400 km (with one exception of 200 km) under the assumption of a decaying step function gamma pulse. Hence, shorter rise times and higher peak electric fields would have been obtained under inclusion of lower HOBs.

	$\alpha_R \to \infty$	$\alpha_R = 5\ ns^{-1}$	$\alpha_R = 2\ ns^{-1}$	$\alpha_R = 1\ ns^{-1}$	Ref.3
E_0 (kV/m)	70.0	70.2	69.6	67.6	55.7
α (ns^{-1})	9.47	4.85	2.46	1.33	1.6
β (ns^{-1})	.0348	.0342	.0340	.0330	0.037
E_{pk} (kV/m)	68.3	67.3	64.8	60.3	50
$(dE/dt)_{pk}$	165	84.5	42.2	21.9	21.8
T_r (ns)	.45	.86	1.65	2.94	2.46
W_∞ (J/m^2)	.185	.188	.184	.175	.107
I_∞ (Vs/m)	2.01×10^{-3}	2.05×10^{-3}	2.05×10^{-3}	2.05×10^{-3}	1.51×10^{-3}

Table VI: Worst case QEXP fits for different Rossi-alphas of the gamma source function compared to the data recommended by C.E. Baum [3]

β, $T_{1/2}$, W_∞ and I_∞ are practically independent of α_R whereas E_{pk} is slightly decreasing with α_R. Again, the energy fluence W_∞ is overestimated with respect to the worst case values shown in Table II.

The worst case QEXP fit derived in the present paper provides a stronger threat then Ref.3 because of the consideration of lower and higher HOBs and a systematic search for maximum values of the various HEMP characteristics.

To specify a 'reasonable' more relieved HEMP standard one could exclude the lowest HOBs (<100km) where E_{pk}, W_∞ and I_∞ are smaller then the maximum values and furthermore cut off the highest value of E_{pk} and $(dE/dt)_{pk}$. As shown by Fig. 17, E_{pk} could be reduced to 87% and $(dE/dt)_{pk}$ to 60% of their maximum values if only 5% of the total coverage area (given by the tangent radium) are omitted.

Then, $E_{pk} \approx 60$ kV/m and $(dE/dt)_{pk} \approx 35$ kV/m/ns are assumed to provide a 'reasonable' set of data. The corresponding QEXP parameters then look as follows

$$E_0 = 64.7 \text{ kV/m}$$
$$\alpha = 2.20 \times 10^9 \text{ s}^{-1}$$
$$\beta = 3.24 \times 10^7 \text{ s}^{-1}$$

which result in

$$E_{pk} = 60 \text{ kV/m}$$
$$(dE/dt)_{pk} = 35 \text{ kV/m/ns}$$
$$T_r = 1.9 \text{ ns}$$
$$T_{1/2} = 23.8 \text{ ns}$$
$$W_\infty = 0.167 \text{ J/m}^2$$
$$I_\infty = 0.002 \text{ Vs/m}$$

ANNEX A

Properties of the QEXP Function

The quotient of the sum of two exponentials (QEXP) is considered to be a sufficiently simple analytic expression to describe the time dependency of the gamma source and a standard EMP wave form as well. The exponential rise of the QEXP reflects the energy release of a nuclear weapon more appropriately than e.g. the widely used difference of two exponentials (DEXP). Whereas DEXP shows a discontinuous derivative at $t = 0$, QEXP is continuously differentiable for all times $-\infty < t < +\infty$. A potential disadvantage of QEXP is its infinite number of poles in the complex frequency plane where DEXP has only two poles. Further properties of these two canonical EMP wave forms are summarized in [4, 5].

In the following, the QEXP function will be considered in its general form

$$E(t) = \frac{1}{e^{-\alpha t}/A + e^{\beta t}/B}. \tag{A.1}$$

For $\alpha \to \infty$, the decaying step function DSF is obtained from Eq. (A.1) used in [2] as a hypothetical gamma source.

By means of the transformation

$$A = E_0 e^{-\alpha t_0}, \qquad B = E_0 e^{\beta t_0}$$

$$E_0 = A\left(\frac{B}{A}\right)^{\frac{\alpha}{\alpha+\beta}}, \qquad t_0 = -\frac{1}{\alpha+\beta}\ln\frac{A}{B}$$

Eq.(A.1) can be transformed to

$$E(t) = \frac{E_0}{e^{-\alpha(t-t_0)} + e^{\beta(t-t_0)}}. \tag{A.2}$$

Because t_0 denotes only a shift of the time scale, for most applications $t_0 = 0$ can be postulated.

E(t) takes its maximum value

$$E_{pk} = E_0\left(\frac{\alpha}{\beta}\right)^{\frac{\alpha}{\alpha+\beta}}\frac{\beta}{\alpha+\beta} \tag{A.3}$$

at the time

$$t_{pk} = \frac{1}{\alpha+\beta}\ln\frac{\alpha}{\beta} + t_0. \tag{A.4}$$

If the condition $\alpha >> \beta$ holds which is normally the case for QEXP fits to calculated EMP fields, the maximum rise (i.e. point of inflection) is obtained at the time

$$\begin{aligned} t_I &= -\frac{1}{\alpha+\beta}\ln\left(1+4\frac{\beta}{\alpha}+\frac{\beta^2}{\alpha^2}+O(\beta^3/\alpha^3)\right) \\ &= -\frac{4}{\alpha}\frac{\beta}{\alpha}\left(1-\frac{11}{4}\frac{\beta}{\alpha}\right) + O(\beta^3/\alpha^3) \end{aligned} \tag{A.5}$$

for which up to terms of the order of β^2/α^2

$$\begin{aligned} \left(\frac{dE}{dt}\right)_{pk} &\approx \frac{E_0}{4}\alpha\left(1-\frac{\beta}{\alpha}+4\frac{\beta^2}{\alpha^2}\right) \\ E(t_I) &\approx \frac{E_0}{2}\left(1-2\frac{\beta}{\alpha}+\frac{15}{2}\frac{\beta^2}{\alpha^2}\right). \end{aligned} \tag{A.6}$$

Thus, to zeroth order of approximation

$$E(t_I) \approx \frac{1}{2}E_0 \approx \frac{1}{2}E_{pk}. \tag{A.7}$$

More accurately, the times $t_{1/2}$ for which

$$E(t_{1/2}) = \frac{1}{2}E_{pk}$$

are given by

$$t_{1/2} \approx -\frac{1}{\alpha+\beta}\ln\left(2\left(\frac{E_0}{E_{pk}}\right)^{\frac{\alpha+\beta}{\alpha-\beta}}-1\right) \approx -\frac{2}{\alpha+\beta}\frac{\beta}{\alpha}\left(1-\ln\frac{\beta}{\alpha}\right). \tag{A.8}$$

for the rising part and

$$t_{1/2} \approx \frac{1}{\beta}\ln\left(2\frac{E_0}{E_{pk}}\right) \tag{A.9}$$

for the decaying part of the QEXP function.

The total half-width of the QEXP can therefore be approximated by

$$T_{1/2} = \frac{1}{\beta}\left[\ln 2+\frac{\beta}{\alpha}\left(1+\frac{\beta}{\alpha}\right)\left(1-\ln\frac{\beta}{\alpha}\right)+\frac{1}{2}\frac{\beta^2}{\alpha^2}\right] + \frac{1}{\beta}O(\beta^3/\alpha^3) \tag{A.10}$$

Similar calculations can be performed to obtain the rise time T_r (i.e. the time interval between 0.1 E_{pk} and 0.9 E_{pk}) in a third order approximation which is sufficiently accurate for $\alpha/\beta \geq 10$

$$T_r \approx \frac{1}{\alpha+\beta} \ln \frac{\varepsilon_1\left(1+\frac{\beta}{\alpha+\beta}\ln(\varepsilon_1-1)\right)-1}{\varepsilon_2\left(1+\frac{\beta}{\alpha+\beta}\ln(\varepsilon_2-1)\right)-1} \tag{A.11}$$

where $\varepsilon_1 = E_0/(0.1\ E_{pk})$ and $\varepsilon_2 = E_0/(0.9\ E_{pk})$

Fig. A.1 shows some results of an exact numerical calculation of T_r together with the zeroth order approximation Eq. (A.13).

The pulse duration (defined as the pulse-width at $E_{pk}/10$) is given by

$$T_{1/10} \approx \frac{1}{\beta}\ln(\varepsilon_1) + \frac{1}{\alpha+\beta}\ln(\varepsilon_1-1) + \frac{1}{\beta}O(\beta^3/\alpha^3) \tag{A.12}$$

Zeroth-order approximation of Eqs. (A.10) to (A.12) are given by

$$T_r \approx 2\ln 9/\alpha = 4.4/\alpha \tag{A.13}$$

$$T_{1/2} \approx \ln 2/\beta = 0.69/\beta \tag{A.14}$$

$$T_{1/10} \approx \ln 10/\beta = 2.30/\beta. \tag{A.15}$$

Of further interest are the impulse or normalization integral

$$N_0 = \int_{-\infty}^{+\infty} E(t)dt \tag{A.16}$$

and the electromagnetic energy fluence

$$W_\infty = \frac{1}{Z_0}\int_{-\infty}^{+\infty} E^2(t)dt \tag{A.17}$$

if E(t) denotes the electric field strength and $Z_0 = 377\ \Omega$ is the impedance of the vacuum. Eqs. (A.16) and (A.17) can be evaluated analytically be contour integration techniques as in [6] or, more conveniently, taken from appropriate tables.

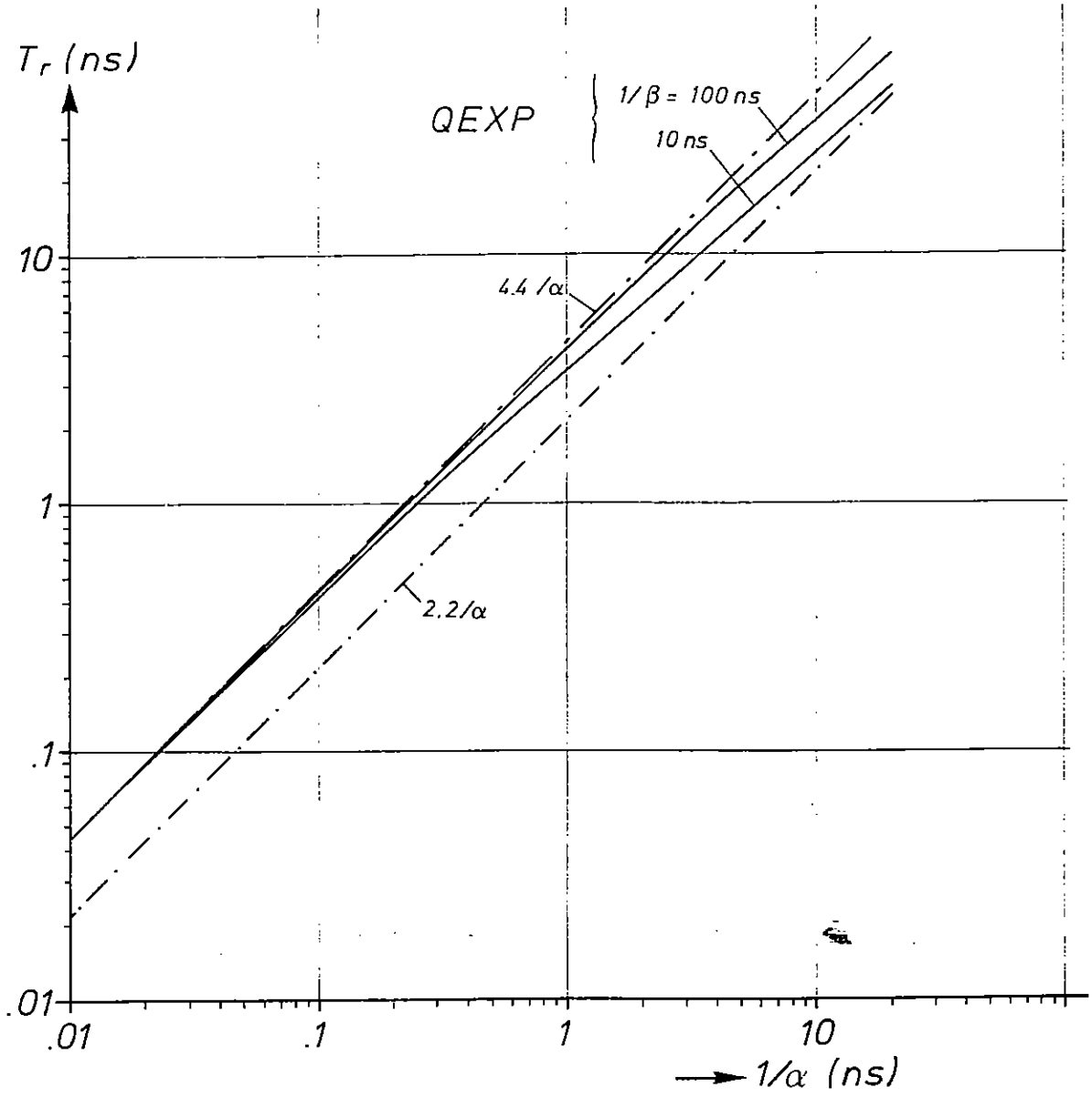

Fig. A.1 Rise time calculated for a QEXP function as a function of $1/\alpha$ together with the approximation Eq. (A.13).

According to [7], the exponential Fourier transform of Eq. (A.2) is obtained as follows

$$\begin{aligned} \tilde{E}(\omega) &= \mathcal{F}(E(t)) = E_0 \mathcal{F}\left(\frac{e^{-\beta t}}{e^{-(\alpha+\beta)t}+1}\right) \\ &= \frac{\pi E_0}{\alpha+\beta} \csc\left(\frac{\alpha-i\omega}{\alpha+\beta}\pi\right). \end{aligned} \tag{A.18}$$

For $\omega = 0$.

$$N_0 = \int_{-\infty}^{+\infty} E(t)dt = E(\omega=0) = \frac{\pi E_0}{\alpha+\beta} \csc\frac{\alpha\pi}{\alpha+\beta}. \tag{A.19}$$

If $\alpha >> \beta$ is satisfied.

$$N_0 \approx \frac{E_0}{\beta}\left(1+\frac{\pi^2}{6}\frac{\beta^2}{\alpha^2}-\frac{\pi^2}{3}\frac{\beta^3}{\alpha^3}+.....\right). \tag{A.20}$$

Similarly,

$$\begin{aligned} \mathcal{F}(E^2(t)) &= \pi E_0^2 \mathcal{F}\left(\frac{e^{-2\beta t}}{\left(e^{-(\alpha+\beta)}\right)^2}\right) \\ &= -\pi E_0^2 \frac{\alpha-\beta-i\omega}{(\alpha+\beta)^2} \csc\left(\frac{2\alpha-i\omega}{\alpha+\beta}\pi\right) \end{aligned} \tag{A.21}$$

Taking $\omega = 0$, one obtains the energy fluence

$$W_\infty = -\frac{\pi}{Z_0} E_0^2 \frac{\alpha-\beta}{(\alpha+\beta)^2} \csc\frac{2\alpha\pi}{\alpha+\beta}. \tag{A.22}$$

If again $\alpha >> \beta$

$$W_\infty \approx \frac{1}{Z_0}\frac{E_0^2}{2\beta}\left(1-2\frac{\beta}{\alpha}+2\frac{\beta^2}{\alpha^2}\left(1+\frac{\pi^2}{3}\right)-\frac{\beta^3}{\alpha^3}\left(1+\frac{4\pi^2}{3}\right)+...\right). \tag{A.23}$$

From Eq. (A.18) one can immediately obtain the amplitude of the electric field in the frequency domain

$$\begin{aligned} \left|\tilde{E}(\omega)\right| &= +\sqrt{E(\omega)E^*(\omega)} \\ &= \frac{E_0}{\alpha+\beta} \frac{\pi}{\sqrt{\sin^2\left(\frac{\alpha\pi}{\alpha+\beta}\right)+\sinh^2\left(\frac{\omega\pi}{\alpha+\beta}\right)}} \end{aligned} \tag{A.24}$$

and the phase angle

$$\begin{aligned} \tan(\varphi+\omega t_0) &= \frac{\mathrm{Im}\,E(\omega)}{\mathrm{Re}\,E(\omega)} = \frac{1}{i}\frac{E(\omega)-E^*(\omega)}{E(\omega)+E^*(\omega)} \\ &= \cot\left(\frac{\alpha\pi}{\alpha+\beta}\right) \tanh\left(\frac{\omega\pi}{\alpha+\beta}\right). \end{aligned} \tag{A.25}$$

In the low-frequency limit

$$\left|\tilde{E}(\omega)\right| \approx \int_{-\infty}^{+\infty} E(t)dt = \frac{E_0}{\alpha+\beta}\frac{\pi}{\sin\frac{\alpha\pi}{\alpha+\beta}}. \tag{A.26}$$

If $\alpha >> \beta$,

$$\left|\tilde{E}(\omega)\right| \approx \frac{E_0}{\beta}. \tag{A.27}$$

For higher frequencies and for $\alpha >> \beta$, respectively,

$$\left|\tilde{E}(\omega)\right| \approx \frac{E_0}{\alpha}\frac{\pi}{\sinh\frac{\omega\pi}{\alpha}} \tag{A.28}$$

which in the high-frequency limit ($\omega \to \infty$) results in

$$\left|\tilde{E}(\omega)\right| \approx \frac{2\pi E_0}{\alpha} e^{-\frac{\omega\pi}{\alpha}}. \tag{A.29}$$

Again assuming $\alpha >> \beta$, the two approximations (A.27) and (A.28) become identical for $\omega \approx \beta$. From the exact spectral function (A.24)

$$\left|E(\omega=\beta)\right| \approx \frac{E_0}{\sqrt{2\beta}} \tag{A.30}$$

is obtained.

Finally, the spectral energy fluence

$$|W(\omega)| = \frac{\pi E_0^2}{Z_0(\alpha+\beta)^2}\sqrt{\frac{(\alpha-\beta)^2+\omega^2}{\sin^2\frac{2\alpha\pi}{\alpha+\beta}+\sinh^2\frac{\omega\pi}{\alpha+\beta}}} \qquad (A.31)$$

can be derived from Eq. (A.21).

Annex B

Variation of Worst Case EMP Parameters with Yield and Gamma Energy

In Sections 4 and 5, the heights of burst and observer positions were determined which maximize the four characteristic quantities E_{pk}, $(dE/dt)_{pk}$, W_∞ and I_∞. The calculations were based on a nominal gamma yield Y_γ = 10 kt and nominal energy of gamma quanta of E_γ = 2 MeV [2].

Fig. B.1 shows the influence of a variation of Y_γ on the four maximum quantities Q_i (i = 1 to 4) normalized for Y_γ = 10 kt. In the yield range 10 to 100 kt there is a further increase of maximum peak rate of rise (by about 30%) and peak electric field (by about 20%), whereas W_∞ and I_∞ saturate (< 10%).

Fig. B.2 is a corresponding plot for the variation of E_γ normalized for E_γ = 2 MeV. In particular, the maximum peak rate of rise shows a considerable increase even above E_γ = 8 MeV, whereas W_∞ and I_∞ decrease for energies greater 3 to 4 MeV. However, it seems to be unlikely that a 10 kt monoenergetic source of such high gamma energies is realistic. Hence, the potential increase of the maxima of $(dE/dt)_{pk}$ and E_{pk} will by much less dramatic than suggested by Fig. B.2 if more realistic spectral distributions of source gammas are considered.

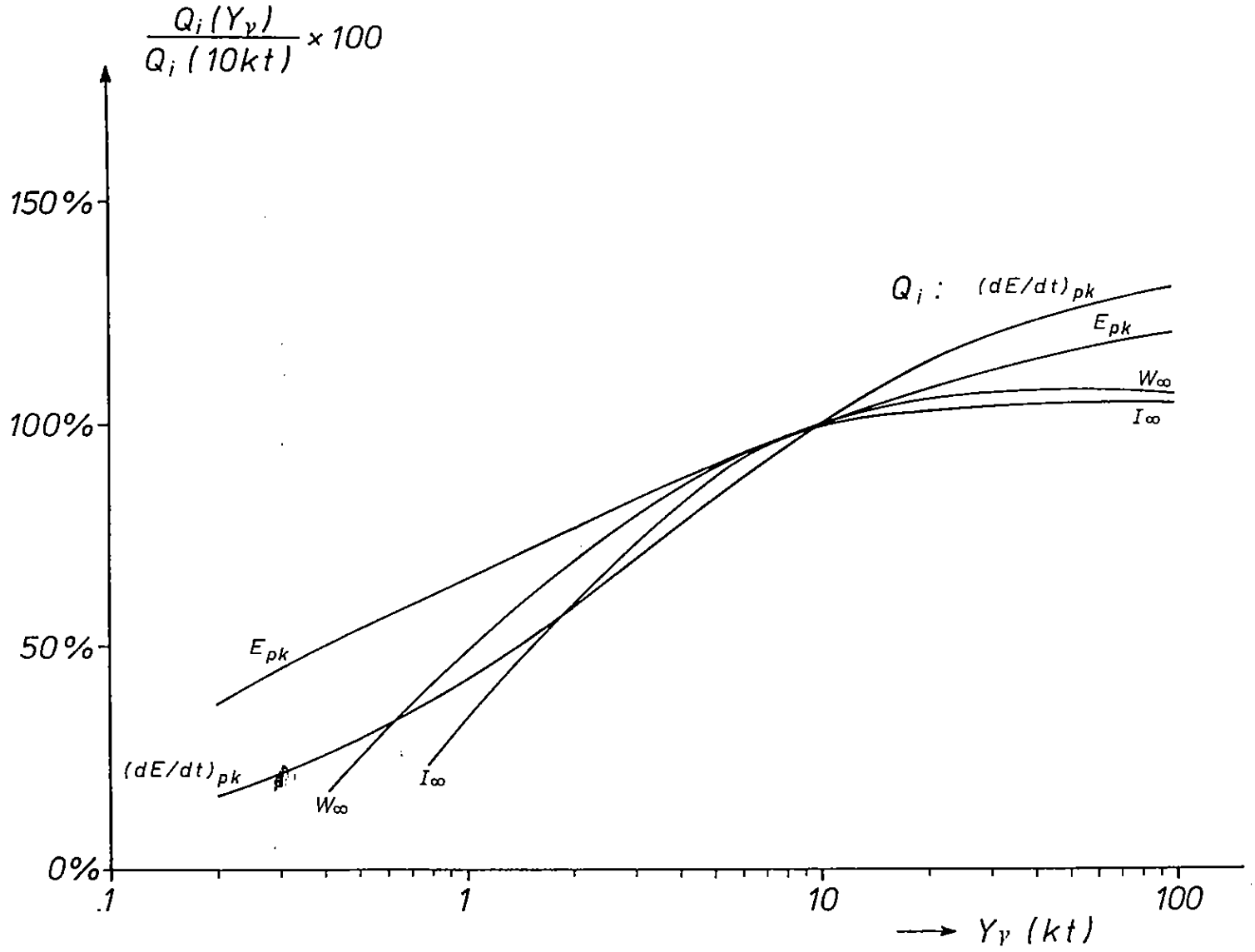

Fig. B.1: Variation of the four maximum quantities Q_i with gamma yield Y_γ normalized at $Y_\gamma = 10$ kt.

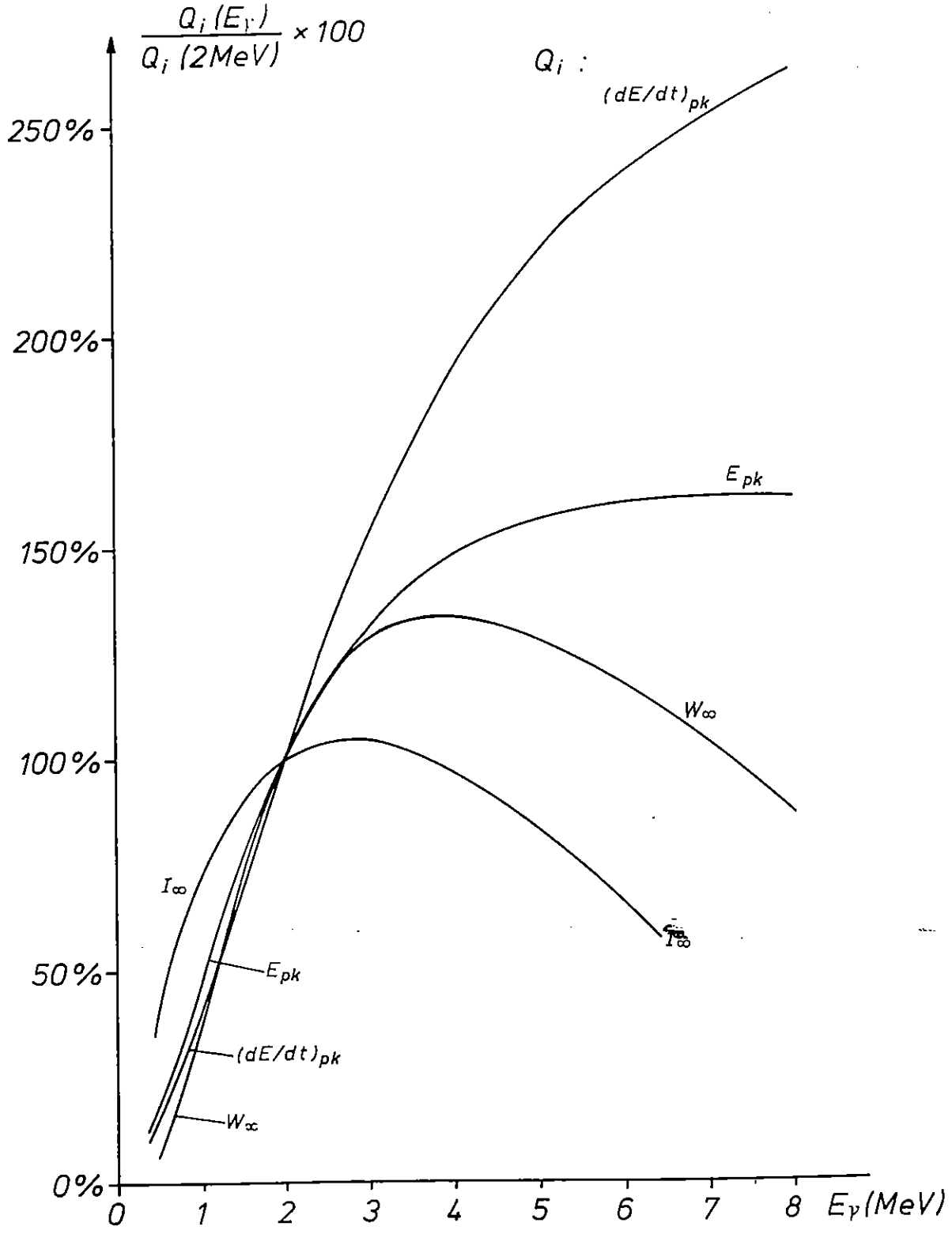

Fig. B.2: Variation of the four maximum quantities Q_i with the energy E_γ of source gammas normalized at $E_\gamma = 2$ MeV.

References

1. K.-D. Leuthäuser, A Complete EMP Environment Generated by High-Altitude Nuclear Bursts, TN 363, 1992

2. C.L. Longmire et al., A Nominal Set of High-Altitude EMP Environments, TN 354, 1987, and ORNL/Sub/86-18417/1, 1987

3. C.E. Baum, From the Electromagnetic Pulse to High Power Electromagnetics, Proceedings of the IEEE, Vol.80, No 6, p.789, June 1992

4. C.E. Baum, Some Consideration Concerning Analytic EMP Criteria waveforms, TN 285, 1976

5. K.S.H. Lee (ed.), EMP Interaction: Principles, Techniques and Reference Data, Hemisphere Publ. Corp., 1986

6. K.-D. Leuthäuser: Reflexion und Transmission von NEMP-Feldern, INT Report Nr. 120, 1985

7. A. Erdélyi (ed.), Tables of Integral Transforms, Vol. I, p.120, McGraw-Hill Book Comp., 1954